SAND2024-07060R

SHASTA
Subsurface Hydrogen Assessment, Storage, and Technology Acceleration

Quantitative Risk Assessment Examples for Aboveground Leaks for an Underground Hydrogen Storage System

SHASTA: Subsurface Hydrogen Assessment, Storage, and Technology Acceleration Project

June 2024

Prepared for the U.S. Department of Energy, Office of Fossil Energy and Carbon Management by:

Sandia National Laboratories: Melissa S. Louie and Brian D. Ehrhart

U.S. DEPARTMENT OF ENERGY | Fossil Energy and Carbon Management

NATIONAL ENERGY TECHNOLOGY LABORATORY · Pacific Northwest NATIONAL LABORATORY · Lawrence Livermore National Laboratory · Sandia National Laboratories · National Nuclear Security Administration

Disclaimer

This report was prepared as an account of work sponsored by an agency of the United States Government. Neither the United States Government nor any agency thereof, nor any of their employees, makes any warranty, express or implied, or assumes any legal liability or responsibility for the accuracy, completeness, or usefulness of any information, apparatus, product, or process disclosed, or represents that its use would not infringe privately owned rights. Reference therein to any specific commercial product, process, or service by trade name, trademark, manufacturer, or otherwise does not necessarily constitute or imply its endorsement, recommendation, or favoring by the United States Government or any agency thereof. The views and opinions of authors expressed therein do not necessarily state or reflect those of the United States Government or any agency thereof.

Additionally, neither National Technology and Engineering Solutions of Sandia, LLC, nor any of their employees makes any warranty, expressed or implied, or assumes any legal liability or responsibility for the accuracy, completeness, or usefulness of any information, apparatus, product, or process disclosed, or represents that its use would not infringe privately owned rights. Reference herein to any specific commercial product, process, or service by trade name, trademark, manufacturer, or otherwise does not necessarily constitute or imply its endorsement, recommendation, or favoring by National Technology and Engineering Solutions of Sandia, LLC. The views and opinions of authors expressed herein do not necessarily state or reflect those of National Technology and Engineering Solutions of Sandia, LLC and should not be used for advertising or product endorsement purposes.

Suggested Citation: Melissa S. Louie and Brian D. Ehrhart, *Quantitative Risk Assessment Examples for Aboveground Leaks for an Underground Hydrogen Storage System,* SAND2024-07060R U.S. Department of Energy SHASTA Project, Sandia National Laboratories, 2024.

SAND2024-07060R

Quantitative Risk Assessment Examples for Aboveground Leaks for an Underground Hydrogen Storage System

SHASTA: Subsurface Hydrogen Assessment, Storage, and Technology Acceleration Project

June 2024

Prepared for the U.S. Department of Energy, Office of Fossil Energy and Carbon Management by:

Sandia National Laboratories: Melissa S. Louie and Brian D. Ehrhart

Executive Summary

Hydrogen energy storage can be used to achieve goals of national energy security, renewable energy integration, and grid resilience. Adapting underground natural gas storage facility (UNGSF) infrastructure for underground hydrogen storage (UHS) is one method of storing large quantities of hydrogen that has already largely been proven to work for natural gas. There are currently some underground salt caverns in the United States that are being used for hydrogen storage by commercial entities, but it is still a fairly new concept in that it has not been widely deployed nor has it been done with other geologic formations like depleted hydrocarbon reservoirs. Assessments of UHS systems can help identify and evaluate risks to people both working within the facility and residing nearby. This report provides example risk assessment methodologies and analyses for generic wellhead and processing facility configurations, specifically in the context of the risks of unintentional hydrogen releases into the air. Assessment of the hydrogen containment in the subsurface is also critically important for a safety assessment for a UHS facility, but those geomechanical assessments are not included in this report.

First, individual risk was calculated for each wellhead configuration and processing facility within an area encapsulating 100 meters directly in front of a leak and 50 meters perpendicular to the leak in either direction. This study was used to compare the contributions of different physical effects to overall risk, including the risks of jet fires compared to explosions, the wellhead compared to the processing facility, and different wellhead configurations compared to each other.

Second, societal risk was calculated for a 50 m by 50 m area of interest located 20 meters away from the leak as an example of a potentially affected area in which people outside of the facility might reside. This analysis revealed results such as which components in the wellhead leaked the most and which facility (wellhead vs. processing facility) posed the greater societal risk. There is also discussion regarding how this societal risk assessment could be used as a general template for assessments conducted for facilities and locations, but more information on local population densities would improve the accuracy of the risk assessment.

Third, a sensitivity study was conducted to discern impacts of different scenarios on overall risk. The varied inputs included modeling parameters and ambient conditions such as the Mach flame speed, ambient temperature, and relative humidity. The Mach flame speed showed an impact on the overpressure risk while the ambient temperature showed a noticeable effect on the heat flux risk and the relative humidity did not seem to greatly influence the heat flux risk.

Finally, an analysis of different physical parameters related to well leaks was conducted to understand the time-dependent aspects of damage that a leak can inflict on infrastructure both within the facility and in the surrounding community. The analysis included an examination of pressure, leak flow rate, jet fire flame length, and jet fire heat flux over space and time, for a range of leak sizes.

The analyses shown in this report can be helpful for identifying potential areas for further study within the UHS risk landscape and for presenting examples of methodologies that can help safely design more specific facilities. The results from these types of risk analyses can be informative to stakeholders such as owner-operators, regulatory bodies, codes and standards organizations, and the broader public.

Acknowledgments

This work was supported by the U.S. Department of Energy, Office of Fossil Energy and Carbon Management (FECM) through the Subsurface Hydrogen Assessment, Storage, and Technology Acceleration (SHASTA) project. The authors would like to thank Mathew Ingraham, Franek Hasiuk, and Donald Conley from Sandia National Laboratories for their technical support, as well as Evan Frye from the U.S. Department of Energy FECM Office of Resource Sustainability, Mathew Ingraham, Dusty Brooks, Kristin Hertz, and Marina Miletic from Sandia National Laboratories, and Angela Goodman from the National Energy Technology Laboratory for their reviews of this document.

This work was performed under the auspices of the U.S. Department of Energy's National Nuclear Security Administration by Sandia National Laboratories. Sandia National Laboratories is a multi-mission laboratory managed and operated by National Technology and Engineering Solutions of Sandia, LLC, a wholly owned subsidiary of Honeywell International, Inc., for the U.S. Department of Energy's National Nuclear Security Administration under contract DE-NA-0003525.

Acronyms and Abbreviations

AGA	American Gas Association
BOP	blowout preventer
DHSV	downhole safety valve
HyRAM+	Hydrogen Plus Other Alternative Fuels Risk Assessment Models
IOGP	International Association of Oil & Gas Producers
MFS	Mach flame speed
NFPA 2	National Fire Protection Association Hydrogen Technologies Code
P&ID	piping and instrumentation diagram
QRA	quantitative risk assessment
SHASTA	Subsurface Hydrogen Assessment, Storage, and Technology Acceleration
SSSV	subsurface safety valve
UHS	underground hydrogen storage
U.K. HSE	United Kingdom Health and Safety Executive
UNGSF	underground natural gas facility

Contents

Executive Summary ii
Acknowledgments iii
Acronyms and Abbreviations iv
1.0 Introduction 1
2.0 Methods 2
2.1 HyRAM+ Methodology and Assumptions 2
2.1.1 Societal Risk 3
2.2 Sensitivity Study 5
2.3 Temporal Leak Analysis 7
3.0 Data Sources 9
3.1 Wellhead 9
3.1.1 Depleted Hydrocarbon Reservoir Operations 9
3.1.2 Salt Cavern Operations 11
3.1.3 Wellhead Entry 11
3.2 Aboveground Processing Facility 12
4.0 Results and Discussion 13
4.1 Individual Risk Results 13
4.2 Societal Risk Results 17
4.3 Sensitivity Study 20
4.3.1 Mach Flame Speed 20
4.3.2 Ambient Conditions 22
4.3.3 Underground Storage Conditions 24
4.4 Temporal Leak Analysis 25
5.0 Conclusion 30
6.0 References 32
Appendix A. Current Subsurface Hydrogen Storage Landscape 34
Appendix B. Risk Assessment Inputs and Data 35
Appendix C. Risk Assessment Inputs and Data 36
Appendix D. Mesh Size Study for Societal Risk Calculations 45
Appendix E. Risk Assessment Results 47

Figures

Figure 2-1. Individual risk assessment methodology flow diagram. 2
Figure 2-2. Birds-eye view showing area of interest and calculation points used in this study..... 4
Figure 2-3. Number of UNGSFs in the United States binned by county population density. 5
Figure 3-1. Depleted hydrocarbon reservoir well configurations used in this report. Reservoir configurations are named R1, R2, and R3 (left to right) [5]. 9
Figure 3-2. Diagrams showing potential leak pathways through each reservoir configuration [5]. 10
Figure 3-3. Salt cavern well configurations used in this report. Cavern configurations are named C1, C2, and C3 (left to right) [5]. 11
Figure 3-4. Generic piping and instrumentation diagram for aboveground processing facility. 12
Figure 4-1. Annual individual risk for a person near an underground reservoir wellhead (excluding processing facility) for configuration a) R1, b) R2, and c) R3. 13
Figure 4-2. Annual individual risk for a person near an underground cavern wellhead (excluding processing facility) for configuration a) C1, b) C2, and c) C3. 14
Figure 4-3. Annual individual risk for a person near the R1 wellhead and processing facility. 15
Figure 4-4. Heat flux contours for a jet flame from a leak that is a) 0.01%, b) 0.1%, c) 1%, d) 10%, and e) 100% of the pipe cross-sectional area (7-inch diameter pipe). 16
Figure 4-5. F-N curves showing societal risk for the area of interest with a population density of 2700 people per square mile for a) R1, b) R2, and c) R3. 18
Figure 4-6. F-N curves showing societal risk for the area of interest with a population density of 2700 people per square mile for a) C1, b) C2, and c) C3. 19
Figure 4-7. a) Individual risk contour for flame speeds of a) Mach 0.35 (default) and b) Mach 5.2..... 20
Figure 4-8. Contour showing difference in individual risk with flame speeds of Mach 5.2 and 0.35. 21
Figure 4-9. Individual risk directly in front of leak for default (0.35) and higher (5.2) Mach flame speed. 22
Figure 4-10. Individual risk contour using a) default ambient conditions (20°C and 89% humidity), b) example ambient conditions for summer in Beaumont, TX (44°C and 52% humidity)..... 22
Figure 4-11. Contours showing difference in individual risk between default ambient conditions (20°C and 89% humidity) and a) Beaumont, TX summertime case (44°C and 52% humidity), b) Charleston, SC summertime case (32°C and 90% humidity), c) St. Clair, MI wintertime case (-18°C and 60% humidity), and d) Allegany, NY wintertime case (-19°C and 89% humidity)..... 23
Figure 4-12. Individual risk directly in front of leak for different ambient conditions..... 24
Figure 4-13. Wellhead pressure for the full duration of a blowout..... 25
Figure 4-14. Release rate of hydrogen from leak for the full duration of a blowout. 26
Figure 4-15. Jet fire visible flame length for the full duration of a blowout..... 27
Figure 4-16. Heat flux contours for the steady-state jet fire from a 2 mm (left), 18 mm (middle), and 180 mm (right) diameter leak. Heat flux levels are taken from HyRAM+ default levels. 27
Figure B-1. Complete fault tree for leak pathways in wellhead configuration R1, including releases into the subsurface..... 37

Figure B-2. Fault tree for configuration R1. 38
Figure B-3. Fault tree for configuration R2. 39
Figure B-4. Fault tree for configuration R3. 39
Figure B-5. Fault tree for configuration C1. 40
Figure B-6. Fault tree for configuration C2. 40
Figure B-7. Fault tree for configuration C3. 40
Figure B-8. Frequency of well entries for each well configuration by well entry type [5]. 41
Figure B-9. Fault tree for aboveground processing facility. 43
Figure C-10. Area of interest with a sample location a) every 10 m, b) every 5 m, c) every 2.5 m, and d) every 1.25 m. 45
Figure D-11. Overpressure contours for a 0.01% leak (a, b), 0.1% leak (c, d), 1% leak (e, f), 10% leak (g, h), and 100% leak (i, j), where Mach flame speed was set to 0.35 (figures on left) and 5.2 (figures on right). 51
Figure D-12. Heat flux contours for 0.01% leak using a) HyRAM+ default, b) Beaumont, TX summer, c) Charleston, SC summer, d) St. Clair, MI winter, and Allegany, NY winter example ambient conditions. 51
Figure D-13. Heat flux contours for 0.1% leak using a) default, b) Beaumont, TX summer, c) Charleston, SC summer, d) St. Clair, MI winter, and Allegany, NY winter example ambient conditions. 52
Figure D-14. Heat flux contours for 1% leak using a) default, b) Beaumont, TX summer, c) Charleston, SC summer, d) St. Clair, MI winter, and Allegany, NY winter example ambient conditions. 53
Figure D-15. Heat flux contours for 10% leak using a) default, b) Beaumont, TX summer, c) Charleston, SC summer, d) St. Clair, MI winter, and Allegany, NY winter example ambient conditions. 54
Figure D-16. Heat flux contours for 100% leak using a) default, b) Beaumont, TX summer, c) Charleston, SC summer, d) St. Clair, MI winter, and Allegany, NY winter example ambient conditions. 55

Tables

Table 2-1. Risk Assessment Inputs 3
Table 2-2. Ambient Temperatures and Humidities Used in Sensitivity Study 6
Table 4-1. Maximum Individual Risk Results in Area of Interest 17
Table 4-2. Complete Drawdown Time by Leak Size 26
Table 4-3. Damage to Structures and Equipment from Thermal Radiation, taken from [18] 28
Table 4-4. 30-Minute Heat Fluxes Over Distance for Each Leak Size. 28
Table A-1. Current Subsurface Hydrogen Storage Facilities in Salt caverns in the United States 34
Table A-1. Default Ignition Probabilities Used in Risk Assessment [4] 35
Table A-2. Assumptions Used in Risk Assessment 35
Table B-1. Component Summary for Reservoir Wells 36
Table B-2. Component Summary for Cavern Wells 36
Table B-3. Component Count for Aboveground Processing Facility 36
Table B-4. Total Failure Frequency per Component Provided in [5] 37
Table B-5. Percent Error Between Calculated and Reported Total Leak Frequencies by Wellhead Configuration 38
Table B-6. Likelihood of Leaks per Component by Leak Size from [5] 41
Table B-7. Well Entry Failure Rates [5] 42
Table B-8. Breakdown of Well Entry Leak Sizes [5] 42
Table B-9. Annual Frequency of Well Entry Failures by Type and Leak Size 42
Table B-10. Annual Leak Frequency per Component in Aboveground Processing Facility by Size [4] 42
Table B-11. Wellhead Leak Sizes 43
Table B-12. Aboveground Processing Facility Leak Sizes 44
Table C-13. Number of Fatalities in Area of Interest with 2700 People per Square Mile 46
Table C-14. Absolute Difference in Number of Fatalities Between Each Mesh Size and Its Previous Mesh Size 46
Table D-15. Societal Risk Results for Wellhead Operational Leaks 47
Table D-16. Societal Risk Results for Wellhead Entry Leaks 48
Table D-17. Societal Risk Results for Aboveground Processing Facility Leaks 48
Table D-18. Summary of All Sensitivity Study Conditions 49
Table D-19. Sensitivity Study Individual Risk Results in Fatalities per Year at z=0 (Corresponds to Figure 4-12) 49

1.0 Introduction

Increasing the availability of energy storage methods is essential to achieving national energy security and resilience goals. Underground hydrogen storage is currently being pursued as a method to facilitate hydrogen use as a low carbon emitting fuel for applications such as transportation and electricity generation [1]. However, the volumetric density of hydrogen is so low that high pressures, large volumes, or a combination of the two are required to store meaningful amounts of energy. Currently, underground natural gas storage facilities (UNGSFs) throughout the United States [2] are used to store large quantities of natural gas in the subsurface; over 9000 of these facilities currently exist [3]. This method could be replicated for underground hydrogen storage (UHS), which would be advantageous since it would make use of existing infrastructure. Some UHS facilities already exist and have been operating at locations in the United States; information on these subsurface hydrogen storage facilities is provided in Table A-1 in Appendix A. While these existing facilities serve as a proof-of-concept for the efficacy of this storage method, broader adoption of the method may require rigorous safety assessment of UHS sites to ensure that the risks are understood and appropriately addressed or mitigated before it is used more broadly.

The risks addressed in this report are centered around the potential outcomes of an unintended release of hydrogen into the air from a leak in the aboveground components of a generic UHS system, to provide an example methodology for performing risk assessments on more specific systems and analyzing the significance and implications of results. Assessment of the hydrogen containment in the subsurface is also critically important for a safety assessment for a UHS facility, but those geomechanical assessments are not included in this report. This work focuses on the potential risks based on the surface equipment a UHS facility.

2.0 Methods

2.1 HyRAM+ Methodology and Assumptions

The quantitative risk assessment (QRA) methodology used in this report was modeled off of methods described in version 5.1 of the Sandia software Hydrogen Plus Other Fuels Risk Assessment Model (HyRAM+) [4]. The Python backend of HyRAM+ was used to assist in all calculations of individual and societal risk. Figure 2-1 below summarizes the methodology used to calculate individual risk in terms of annual fatality frequency, at coordinates relative to the location and orientation of a hydrogen leak.

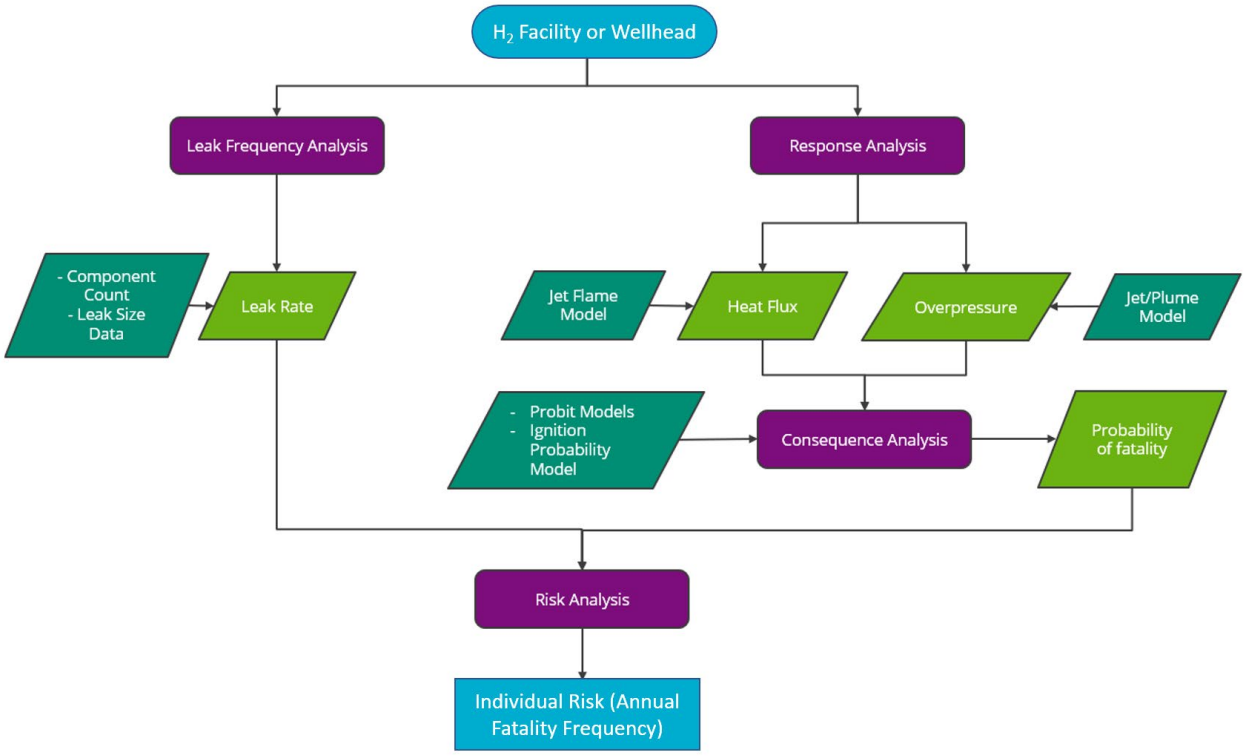


Figure 2-1. Individual risk assessment methodology flow diagram.

The risk assessment was conducted for both the wellhead assembly that connects the underground reservoir or cavern to piping aboveground, and the aboveground facility that filters and compresses the extracted hydrogen before it can be transported to its point of use. Oil and gas wellhead configurations from a risk assessment performed by C-FER Technologies [5] were used to model failures in the wellhead during both normal operations and during wellhead entries for maintenance or monitoring. Since underground hydrogen storage is still an emerging technology, there are few available resources on hydrogen-specific wellhead configurations, but wellhead configurations from the oil and gas industry can be used as a reasonable proxy. This risk assessment provided the component counts, leak pathways, and leak frequency data used in this UHS risk assessment. A generic piping and instrumentation diagram (P&ID) was generated to determine reasonable component counts for the aboveground processing facility, and the fault tree with component leak frequency data from HyRAM+ [4] were used to model these processing facility failures. The failure frequencies and the fault trees from which they were derived are provided in Appendix C.2 for both the wellhead and the processing facility. The leak sizes for both facilities can also be found in the same appendix.

It was assumed that the hydrogen leak was always directly horizontal, and that the affected people and infrastructure in the area of interest were on the same horizontal plane; topographical data or considerations such as multi-stored buildings were not included in the calculations. This conservative assumption meant that each calculation showed the maximal damage that could be inflicted on the people and infrastructure by an ignition event, since any nonzero angle between the leak and the plane of the people and buildings would decrease the horizontal reach of damaging heat flux and overpressure.

A list of inputs used for the risk assessment is shown in Table 2-1 below. The wellhead configurations are described in Sections 3.1.1 and 3.1.2 while the processing facility is detailed in Section 3.2. The Mach flame speed and ambient conditions were chosen based on defaults in HyRAM+. These values were varied in a sensitivity study and are described in detail in Section 2.2.

Table 2-1. Risk Assessment Inputs

Variable	Input
Wellhead Fuel Temperature	80°C (176°F)
Wellhead Fuel Pressure	3×10^7 Pa (4350 psi)
Processing Facility Fuel Temperature	20°C (68°F)
Processing Facility Fuel Pressure	6.9×10^6 Pa (1000 psi)
Mach flame speed	Mach 0.35
Ambient Temperature	20°C (68°C)
Ambient Pressure	1×10^5 Pa (14.5 psi)
Relative Humidity	89%

While blends of hydrogen and hydrocarbon-based fuels like natural gas are possible alternatives or interims for pure hydrogen, the scope of this project is focused on the storage of pure hydrogen. In addition, if the end use for underground-stored hydrogen were in the form of a blended fuel, the blending would likely happen at the surface after cleaning and processing of the hydrogen; the blended fuel would not be stored underground and processed altogether.

2.1.1 Societal Risk

The previous section provides an overview of how to calculate individual risk, which is important for personnel within a facility as well as people who are unaffiliated but still live and work within a potentially affected area. Societal risk is a similar metric that allows for an understanding of how many people would be affected by a particular event, based on the population densities in the areas around the UNGSF sites.

Since population density is available on a per-area basis, an area of interest was selected as shown in Figure 2-2 below. The red point at the origin shows a potential leak point and the arrow shows the direction of the leak. The x-direction is horizontal and parallel to the direction of the leak while the z-direction is horizontal and perpendicular to the direction of the leak.

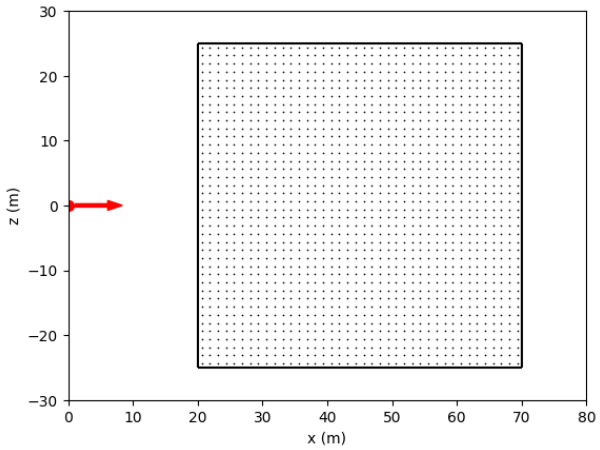


Figure 2-2. Birds-eye view showing area of interest and calculation points used in this study.

It was assumed the facility would be located at least twenty meters away from where any people outside of the facility would be present. The area of interest is therefore twenty meters away from the leak point, and an area of 50 m x 50 m was chosen. The distances and areas in this study were chosen arbitrarily to illustrate the methodology with an example calculation; they are not meant to reflect any specific facility, nor to recommend an area of interest for risk assessments in general. This grid was then split into 1600 cells, evenly spaced out across forty points in 1.25 m intervals in either direction (see Appendix D for the rationale for the choice of spacing in this calculation). Societal risk is often depicted as F-N curves, where the frequency (F) of a certain event is plotted on the y-axis and the predicted number of fatalities (N) resulting from that event is plotted on the x-axis. In this assessment, the frequency of potentially fatal events was calculated using

$$F_{i,j,k} = f_{i,j} \times p'_{\{k|i,j\}} \qquad \text{Equation 2-1,}$$

where f is the frequency of a leak of size i occurring through leak pathway j, and p' is the probability of physical effect k (referring to a jet fire or an explosion) resulting from that leak. The annual frequencies for each component and leak size are provided in Appendix C.2, in addition to fault trees showing the leak pathways considered.

The number of fatalities from each jet fire or explosion event was then calculated using

$$N_{i,j,k} = \sum_{n} p''_{i,j,k,n} \times \rho_{population} \times A_{cell} \qquad \text{Equation 2-2,}$$

where p'' is the probability of fatality for outcome k from leak size i and pathway j at location n (corresponding to each point in Figure 2-2, or the center of each cell), $\rho_{population}$ is the population density (people/area), and A_{cell} is the area of the cell, which was around 1.5 m^2 in this study. Each event frequency, $F_{i,j,k}$, and the corresponding number of fatalities for that event, $N_{i,j,k}$, was plotted as a point on the F-N curve.

Since this risk assessment was done for a generic system rather than one in a specific location, the population density was not defined. A database from the Geospatial Management Office lists UNGSFs across the United States in addition to the counties they are located in [2]. Census data was then used to tabulate county population densities, shown in Figure 2-3 below, since county-level information was the most granular geospatial data included in the database.

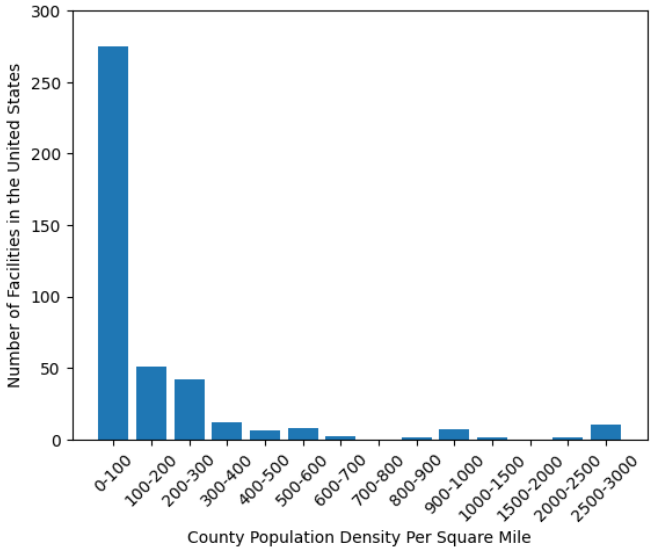


Figure 2-3. Number of UNGSFs in the United States binned by county population density.

In the data set, the county with the highest population density contains around 2700 people per square mile, or around 2.6 people in the 2500 m^2 area of interest shown in Figure 2-2, so this population was used for the assessment. However, county population densities are not always reflective of local population densities since the distribution of where people reside is often not consistent across the county. Given such a small area of interest, it would have been more accurate to understand the spatial layout at a more local level, for example, if there was a neighborhood or school in the vicinity of the UHS system. In the absence this type of information, the highest county population density from the UNGSF dataset was used, but risk assessments of real-life UHS facilities should account for more localized population densities and distributions. Guidance in [6] can be used to determine appropriate population densities for location-specific risk assessments.

Another assumption made for the societal risk calculation was that the leak point was always considered to be at the same location at (0, 0), though in reality all components throughout the wellhead and the processing facility would be spread out over some area so that not all leaks would occur at this origin point. This assumption was made because the system of interest is generic and any spatial data about the facility layout would be speculative. A more detailed risk analysis could take different leak points into account, although a conservative estimate would be to assume that all leaks occur at the leak point closest to the population that may be harmed. This simplified version of the layout also leads to a conservative estimate of societal risk since the population is centered about the leak in the z-direction.

2.2 Sensitivity Study

A sensitivity study of several input variables was conducted to compare their effects on risk and to show potential methods for visualizing these impacts.

The first variable considered was the Mach flame speed of a leaking plume. The Mach flame speed is a measure of how quickly the flame front propagates through an unignited flammable mixture of gas; higher Mach flame speeds can lead to more severe and far-reaching overpressure effects, which in turn increases individual risk for people within the affected area. The value of the Mach flame speed is influenced by the fuel properties and amount of congestion or confinement present near a leak point. Congestion is created by obstacles such as piping and instrumentation in the system or even other objects such as vehicles or vegetation that may be nearby. When the flow of an unignited plume of hydrogen

encounters these types of obstructions, it increases in turbulence, which facilitates mixing of hydrogen with the surrounding air. This mixing can increase the Mach flame speed of the plume. A leaking hydrogen plume may encounter confinement if there are walls, which create enclosed spaces in which unignited hydrogen can accumulate and mix with the air; this degree of confinement would also increase the Mach flame speed of the plume. Therefore, changing the Mach flame speed can approximate the effects of different amounts of congestion and confinement being present in the system. In addition, in the event of an overpressure outcome, a wall provides a surface that a blast wave can reflect against, which increases the severity of the overpressure effects. While this effect is not necessarily linked to the Mach flame speed of the initial plume, increasing the Mach flame speed in the simulation is a way to account for this behavior. Confinement also has the potential to increase the probability of delayed ignition because the hydrogen accumulates instead of dissipating, but a lack of data on ignition probabilities and confinement as well as the lack of a specific system setup prevented a detailed study on this consideration.

Depending on the location, applicable regulations, and owner-operator preferences, existing oil and gas wellheads and their auxiliary processing equipment in the United States are either located within some sort of enclosure, covered with open sides, or completely unsheltered. Consideration of these variations in protective infrastructure for components that convey hydrogen led to the selection of different potential plume Mach flame speeds. The subsonic HyRAM+ default flame speed of Mach 0.35 was used to represent a low degree of confinement for a wellhead and processing facility located outdoors. A higher, supersonic flame speed of Mach 5.2 was used to represent a system that is in some way confined by an enclosure, where walls or other objects provide a location near where leaked hydrogen can accumulate or an obstacle that increases turbulence in the flow of leaking hydrogen. These two flame speeds were selected from a list of Mach flame speeds from blast curves used in the Baker-Strehlow-Tang (BST) model implementation in HyRAM+ [7]. It should be noted that there are currently no regulations or standards regarding safe building design for hydrogen wellhead infrastructure in particular but that codes such as the National Fire Protection Association Hydrogen Technologies Code (NFPA 2) [8] do offer guidance and limitations on the number, placement, and orientation of barrier and fire protection walls present near hydrogen systems, which is meant to restrict the corresponding overpressure response.

The second aspect considered in the sensitivity study was the combination of ambient conditions. The existing underground natural gas facilities in the United States span a wide range of locations across the country. Four representative locations were chosen to vary the ambient temperature and humidity: the summer in Beaumont, Texas was used to represent high temperature and low humidity, the summer in Charleston, WV was used to represent high temperature and high humidity, the winter in St. Clair, MI was used to represent low temperature and low humidity, and the winter in Allegany, NY was used to represent low temperature and high humidity. Values were chosen using representative 2023 weather data from NOAA [9] as a basis and purposely selecting extreme maximum and minimum values to most obviously show the impacts of ambient conditions on individual risk. Table 2-2 summarizes the conditions used in the sensitivity analysis.

Table 2-2. Ambient Temperatures and Humidities Used in Sensitivity Study

Ambient Condition	**Default Conditions**	**“Hot and Dry” Summer near Beaumont, TX**	**“Hot and Humid” Summer Near Charleston, WV**	**“Cold and Dry” Winter near St. Clair, MI**	**“Cold and Wet” Winter near Allegany, NY**
Temperature (°C)	20	44	32	-18	-19
Relative Humidity (%)	89	52	90	60	89

Finally, the underground storage conditions for hydrogen were varied. Well depth can influence both the temperature and pressure within the well, as can geological considerations like the pressure required to maintain the structural integrity of the reservoir or cavern. Depleted reservoirs may have a pressure range around 7-40 MPa and a temperature of around 65°C (149°F), while salt caverns have a pressure range around 8-30 MPa and a temperature of around 80°C (176°F). Cavern conditions of 30 MPa and 80°C were used as the default conditions in this study (for all reservoir and cavern configurations), and the reservoir conditions of 40 MPa and 65°C were tested in the sensitivity analysis to see how changes in the storage conditions would affect the risk of the wellhead and processing facility to people nearby. Lower ranges of pressures were not considered because high pressures of hydrogen storage are more realistic for storing meaningful quantities of hydrogen.

2.3 Temporal Leak Analysis

Most wells have safety measures in place that are meant to prevent unintended and uncontrolled releases of fluids from the wellhead. Wellhead safety devices include downhole safety valves (DHSVs), also known as subsurface safety valves (SSSVs), and blowout preventers (BOPs), which are all designed to prevent the unintended and uncontrolled release of fuel from the wellhead. Failure of these components can result in catastrophic events, including loss of life, destruction of the wellhead components, and damage to nearby infrastructure. Blowouts in onshore wells can be stopped by initiating a well kill, which involves pumping high density fluids through the wellbore to either increase the friction to flow in the wellbore or to generate enough hydrostatic head above the stored fluids in the well to stop any further upward flow. However, conducting a well kill is not always effective or successful, as was the case in the 2015 Aliso Canyon underground natural gas storage facility leak, during which seven attempts to kill the well from the top of the wellhead failed until an attempt to kill the well at a depth of several thousand feet finally succeeded [10]. In addition to the physical difficulties of effectively stopping a blowout, the process of killing a well can be so costly or dangerous that well owner-operators may voluntarily allow the blowout to occur. The natural gas involved in the Aliso Canyon incident was denser than hydrogen, indicating that killing a hydrogen storage well by pumping in heavy fluids may be easier and more efficacious than stopping a leak in a crude oil or natural gas well. However, it is still critical to consider the possibility of a blowout from a large leak in a hydrogen wellhead. Additionally, while smaller, non-catastrophic leaks are more manageable and unlikely to lead to complete drawdown of a well because they can be detected and repaired, mitigation measures may still take on the order of months. The Aliso Canyon leak was not characterized as a complete blowout, but the release was not contained for 111 days, or almost four months, with a leak quantity of over 100,000 tons of natural gas [10].

In the short-term, the consequences of a jet fire mainly concern human exposures. For example, the default exposure time to a jet fire in HyRAM+ is 30 seconds, which accounts for the time it takes for a person to evacuate the affected area. In the longer-term (on the order of hours or even days), infrastructure vulnerability can become a concern, especially when large quantities of stored fuel are present and continue to contribute to the fire. For example, the Deepwater Horizon release spanned 87 days [11], and within just the first few days the combination of an initial explosion and ongoing fires had led to the collapse of the entire rig. Onshore, there may be even more infrastructure outside of the wellhead facility that is vulnerable to long-lasting fires since damage to buildings increases with time and heat flux emitted by the fire. This blowout study includes analyses of jet fire characteristics including heat flux and flame length over space and time over the course of the leak.

Explosive events like deflagrations and detonations are also affected by large quantities of released fuel. These events occur when flammable mass accumulates and ignites after a delay, so larger storage quantities may potentially cause larger overpressure events that affect longer distances. However, since wellheads are located outdoors and the stored hydrogen would be gaseous and therefore disperse quickly,

especially with the presence of wind, it is unlikely that unignited hydrogen would accumulate in a larger quantity than that present during the steady-state period of a blowout. Thus, the blowout analysis in this report focuses only on the consequences of jet fires.

Leak diameters of 2 mm, 18 mm, and 180 mm for a small, medium, and large leak respectively were examined in the blowout analysis. These were the greatest leak diameters for each leak size category out of all well configurations provided in [5]. Well conditions of 30 MPa and 80°C and a well volume of 900,000 m^3 was assumed, based on the largest hydrogen storage cavern size currently used in the United States (see Table A-1). The ambient pressure was set as 101.325 kPa and the ambient temperature was set as 20°C. For simplicity, hydrogen was used as the cushion gas – all 900,000 m^3 of storage and 30 MPa of pressure was from hydrogen rather than using a different cushion gas like N_2 or CO_2, leading to a calculated stored hydrogen mass of around 15,900 metric tons. A pressure gradient along the depth of the well was not considered. The calculations were conducted using HyRAM+ backend capabilities.

3.0 Data Sources

The following sections describe the data sources and example system configurations used in the risk assessment throughout this report.

3.1 Wellhead

The risk analyses were conducted for two systems in the UHS facility – the wellhead and the aboveground, post-extraction processing facility. The wellhead is comprised of a set of components that connect the underground well to pipelines at the surface. The two types of subsurface formations that can serve as storage wells are depleted hydrocarbon reservoirs and salt caverns. Examples of the different basic wellhead design and components needed for each type of well are shown in the following sections.

It should be noted that UHS is not currently an established industry, so the well configurations, frequency data, and leak size data for both the wellhead [5] and processing facility [4] are based on the oil and gas industry; examples of the original data sources include the American Gas Association (AGA), the International Association of Oil & Gas Producers (IOGP), and Global Reporting Initiative. The wellhead configuration may be slightly fuel-dependent – for example, a hydrogen well might require a different well bore diameter and orientation from a natural gas well – but the overall equipment and especially the aboveground configuration would likely not differ drastically between wells storing different fuels.

The descriptions of wellhead components and activities in the following sections were written based on a combination of internal conversations with oil and gas experts and open-source industry materials such as the Schlumberger Energy Glossary [12].

3.1.1 Depleted Hydrocarbon Reservoir Operations

The existing UHS facilities in the United States are all salt caverns; however, depleted hydrocarbon reservoirs are another geologic formation under consideration for UHS usage that could greatly increase the national hydrogen storage capacity. Three wellhead configurations that can be used for depleted reservoir wells, shown in Figure 3-1, were taken from [5] for the reservoir risk assessment. From left to right, they incorporate more components, with many of the additions such as the packer and DHSV adding layers of protection against leaks and blowouts.

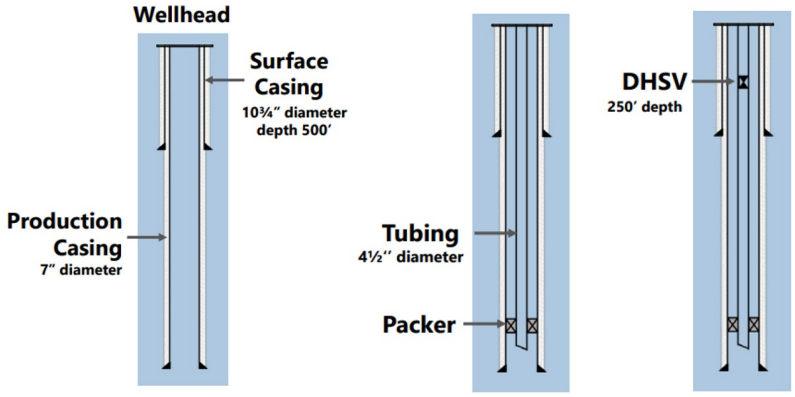


Figure 3-1. Depleted hydrocarbon reservoir well configurations used in this report. Reservoir configurations are named R1, R2, and R3 (left to right) [5].

The surface casing provides a conduit through which fluids can flow and improves structural integrity in the wellbore to prevent collapse of the well. The production casing is used to isolate and protect the production zone and maintain pressure in the event of a leak in the tubing. The tubing provides a pathway for fluids to flow through so the production casing can be protected from reservoir fluids. The packer is used to seal the annular space between the casing and tubing to prevent unintended fluid flow. In the event of an emergency, such as an unintentional flow of fluids out of the wellhead, the DHSV fails in the closed position to seal the wellhead. The components used for the risk assessment of each reservoir wellhead configuration are included in Section C.1.

Operational risk refers to the risk of leaks occurring during everyday operation of the wellhead, and it accounts for all the leak pathways through which hydrogen can travel from the well to the atmosphere outside of the wellhead. As discussed in the HyRAM+ v5.1 Technical Reference Manual, risk can be calculated with a frequency and a consequence [4]. Diagrams showing potential leak pathways through each well configuration, shown in Figure 3-2 and provided in [5], were used to create the fault trees shown in Appendix C.2.1. The blue vertical arrows represent leaks directly from the wellhead to the atmosphere while the green horizontal arrows in the diagrams show leaks from the well into the subsurface. Leaks directly into the atmosphere can pose safety hazards near the facility if they ignite or cause high pressure hydrogen to impinge on surrounding people or infrastructure. Leaks into the subsurface may travel through a porous gas field underground before being released into the atmosphere far from the wellhead facility, which make them difficult to detect and can lead to large undetected losses of product. While both types of leaks are problematic for a UHS facility, this QRA focuses on the safety impacts of leaks directly into the ambient air onsite, so the leak pathways into the subsurface were omitted in this analysis.

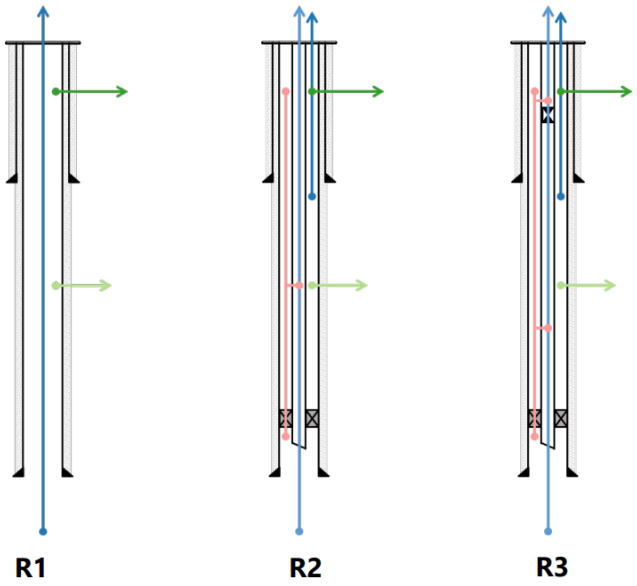


Figure 3-2. Diagrams showing potential leak pathways through each reservoir configuration [5].

In Figure 3-2, the blue arrows show releases into the air out of the wellhead, the green arrows show releases into the subsurface through the casing, and the pink pathways show unintended releases between the internal components of the wellhead assembly, such as through the tubing or the packer. In this report, two types of orifices were considered for an unintended release of stored fuel: wellhead through casing (vertical arrow on the left in the R2 configuration in Figure 3-2) and wellhead through tubing (vertical arrow on the right in the R2 configuration in Figure 3-2). The generated fault trees, marked with the type of orifice each leak pathway terminates in, are shown in Appendix C.2.1. Each orifice type had three

potential leak sizes, characterized by the data source as “small,” “large,” and “rupture.” These orifice sizes were used to determine the magnitude of the jet fire and explosion consequences in the QRA for wellhead operations. The orifice sizes are shown in Appendix C.3.1.

3.1.2 Salt Cavern Operations

The QRA method for the salt cavern configurations was the same as that for the depleted reservoir configurations, except the components and fault trees were slightly different. Three cavern wellhead configurations are shown in Figure 3-3.

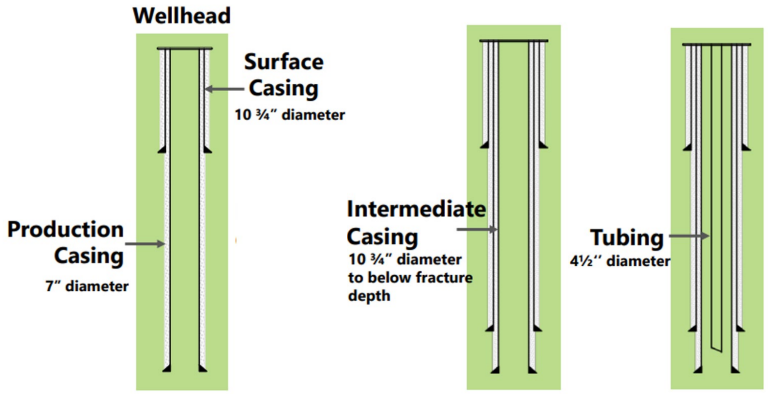


Figure 3-3. Salt cavern well configurations used in this report. Cavern configurations are named C1, C2, and C3 (left to right) [5].

The second two salt cavern configurations contain intermediate casing, which is not present in the depleted reservoir wellhead designs. The intermediate casing provides the wellbore with additional structural integrity and isolation capabilities. The fault trees and leak sizes for the salt cavern configurations can be found in Appendix C.2.1 and Appendix C.3.1 respectively. Unlike the progression of reservoir configurations R1 through R3, the addition of components through cavern configurations C1 through C3 adds more structural integrity to the well but not necessarily more protection against leaks out of the wellhead. In fact, adding intermediate casing between configurations C1 and C2 adds another pathway for a subsurface leak but does not add a pathway for a leak to the atmosphere, so their operational risk profiles were considered to be the same in this analysis.

3.1.3 Wellhead Entry

Besides the risk of leaks from a wellhead during normal operation, there is also the risk of leakage during entry of the well. Well entry can be necessary for routine maintenance and cleaning, or to repair components and monitor well production. Data were available from [5] for workover, coiled tubing, and wireline entries. Workovers are well entry processes that can be used for activities such as cleaning or replacing components within the well or wellhead. Coiled tubing can be used during well entries to circulate fluids to clean the wellhead, extract lost equipment, and transport logging and monitoring tools through the wellhead. Wireline entries refer to processes that involve the lowering of wiring or cables into the well, for the conveyance of maintenance or monitoring tools. Coiled tubing and wireline entries are two types of workovers, but it was assumed that all the provided frequencies were independent of each other and that the workover frequencies represented processes outside of coiled tubing and wireline entries.

The wellhead entry data is shown in Appendix C.2.2. One notable aspect of the data is that the annual frequency of well entries, which dominates the overall well entry leak frequency, increases with complexity and number of components in the well.

Specific leak sizes were not included in [5], so the "wellhead through casing" leak sizes in Appendix C.3.1 were used conservatively since they represented the largest leaks compared to the rest of the orifice types.

3.2 Aboveground Processing Facility

Once a fuel gas is drawn out of a well, it must undergo some processing before being transported elsewhere via a pipeline. This processing step would likely occur within the facility boundaries within which the wellhead is located. A generic piping and instrumentation diagram (P&ID) for processing the hydrogen between the wellhead and the pipeline is shown in Figure 3-4. Once the hydrogen is extracted from the well, filters are used to remove any cushion gas and impurities such as hydrogen sulfide that may have been produced from geochemical or microbial interactions in the well. The gas also must be compressed to the pipeline pressure before exiting the facility. As this is a generic mockup of a processing facility, real facilities may require more equipment specific to their system or different numbers of components. For example, in general, more impurities and contaminants like hydrogen sulfide (H_2S) may be drawn out of a depleted hydrocarbon well than a salt cavern because solution-mined salt caverns tend to be freer of microbial and chemical activity. Thus, the well type could influence the processing facility design by requiring more or fewer filters.

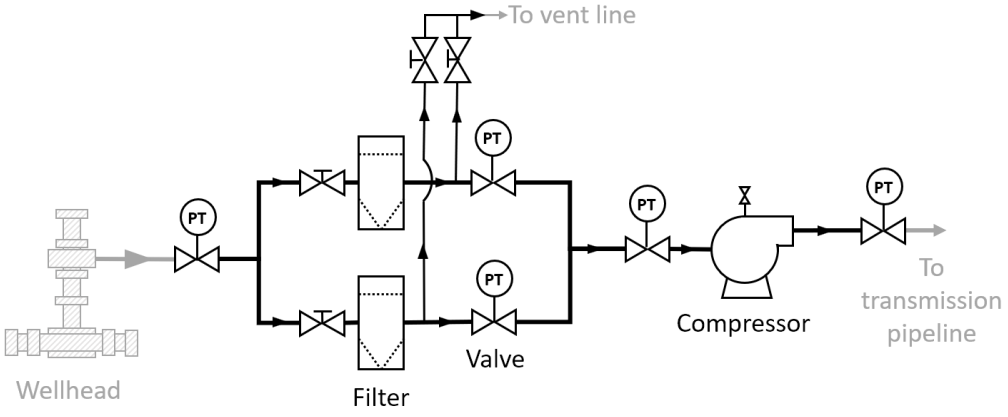


Figure 3-4. Generic piping and instrumentation diagram for aboveground processing facility.

The aboveground processing facility was included in the individual and societal risk calculations described in Section 2.1. The default leak frequencies in HyRAM+ 5.0 were used for all components except for the filter leak frequencies, which are currently under revision. The annual leak frequencies used in the study are provided in Appendix C.2.3. The consequences used in the risk analysis were calculated using the five leak sizes in Table B-12. Natural gas gathering pipelines, used to transport product from a well to a processing plant, tend to have diameters of 100–300 mm. Feeder pipelines for transporting product from a processing facility to longer-range transmission pipelines range from 150–510 mm [13]. A pipe inner diameter of 180 mm (7 in) was used for the piping in the processing facility, both because it fell within these pipeline ranges and because it would have the same leak size as the largest leak in the wellhead data, which allowed for an easier comparison of risk from the wellhead and processing facility. This diameter is also comparable to that used in other UHS risk assessments, such as the study by Portarapillo et al. on the risk posed by a 250-mm pipeline rupture [14].

4.0 Results and Discussion

4.1 Individual Risk Results

Risk to individuals, in terms of the annual frequency of fatality, is an important metric to consider for both people within the site of the wellhead and processing facility as well as those who live or work outside of the facility but may still be within an affected vicinity of a hydrogen leak. Individual risk was calculated for each wellhead configuration in a grid with 0.625 m intervals between each calculation in the x and z directions. The grid spans 100 meters in the x-direction and 50 meters in either z-direction to show how the individual risk changes over a large area. The individual risk results for wellheads with the underground depleted reservoir configurations are shown in Figure 4-1 and the results for wellheads with the underground salt cavern configurations are in Figure 4-2. Both figures only include the wellhead operational risk and well entry risk and exclude the processing facility risk to show the variations in risk from the different wellhead configurations.

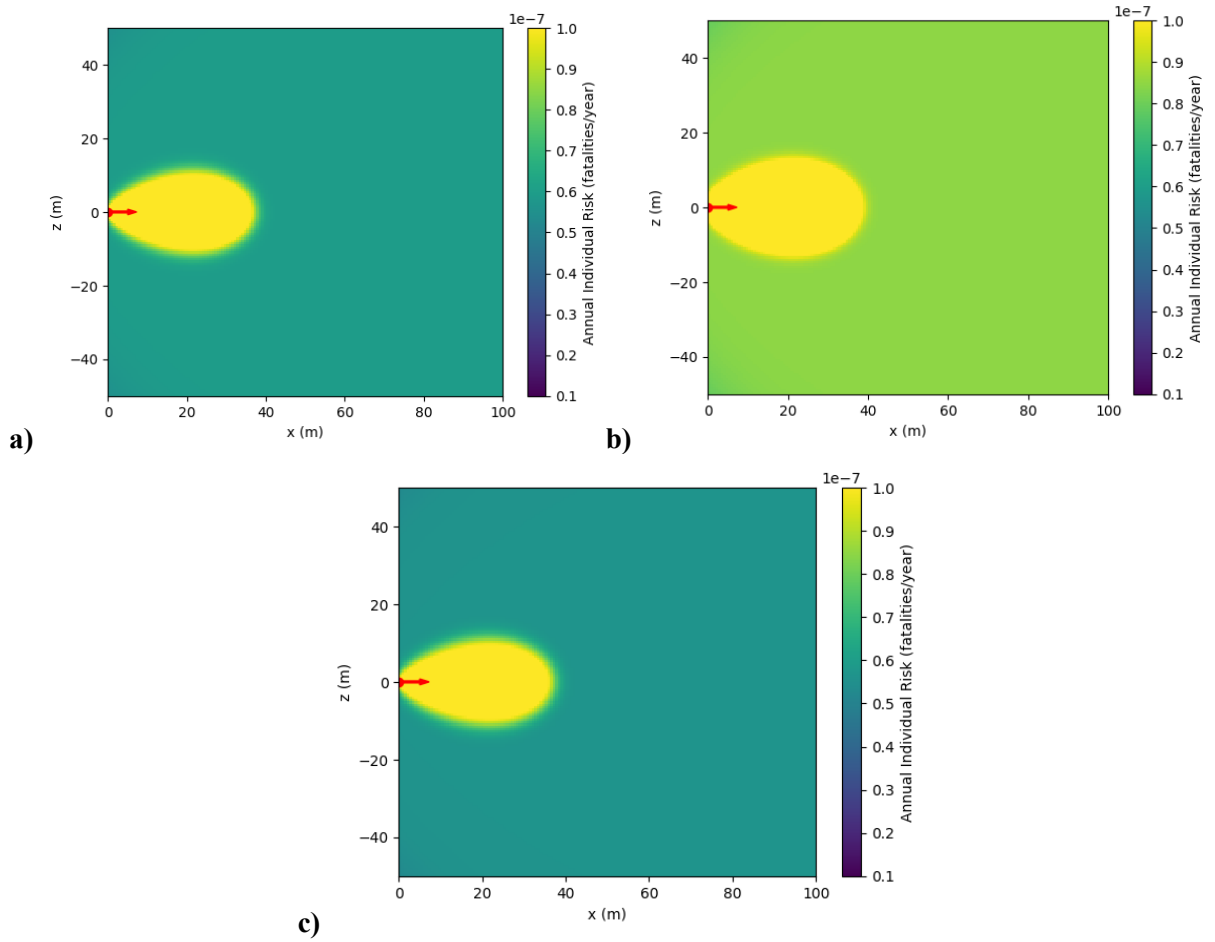


Figure 4-1. Annual individual risk for a person near an underground reservoir wellhead (excluding processing facility) for configuration a) R1, b) R2, and c) R3.

Figure 4-1 shows that all three reservoir wellhead configurations contain a yellow area within which the individual risk is at least a 1×10^{-7} annual probability of fatality; this area reaches roughly 40 meters in front of the leak. Note that this contour mimics the shape of a jet fire out of the leak point more than it mimics the shape of a shock wave from an overpressure event; the overpressure risk is low due to a lower probability of delayed ignition than the probability of immediate ignition, and because of its low Mach

flame speed assumption. Outside of this area of elevated risk and within the area shown, configuration R1 leads to an individual risk of around 6–7×10^{-8} annual fatality frequency, compared to the slightly higher individual risk from configuration R2 of around an 8–9×10^{-8} annual fatality frequency and a slightly lower individual risk from configuration R3 of around a 5–6×10^{-8} individual annual fatality frequency. Configuration R1 only has a single leak pathway, which is through the casing and out of the wellhead (reference Appendix C.2.1 for fault tree visuals). Configuration R2 has two leak pathways, one through the casing and out of the wellhead and one through the tubing and out of the wellhead, which likely accounts for the slightly higher risk profile of R2 compared to R1. Configuration R3 has four leak pathways through the wellhead; however, the inclusion of leak-prevention components such as the packer and DHSV in configuration R3 leads to its slightly lower risk values. Within the area shown, all three reservoir configurations lead to an individual risk within an order of magnitude of 1×10^{-7} fatalities per year.

The individual risk contours for the cavern wellhead configurations are shown in Figure 4-2. Configurations C1 and C2 have the same leak pathway as R1 (through the casing and wellhead to the outside air). Configuration C3 is like R2 in that it has a leak pathway through the casing and wellhead to the air and a pathway through the tubing and wellhead to the air. This additional leak pathway is likely the cause of the slightly higher risk from C3 compared to C1 and C2.

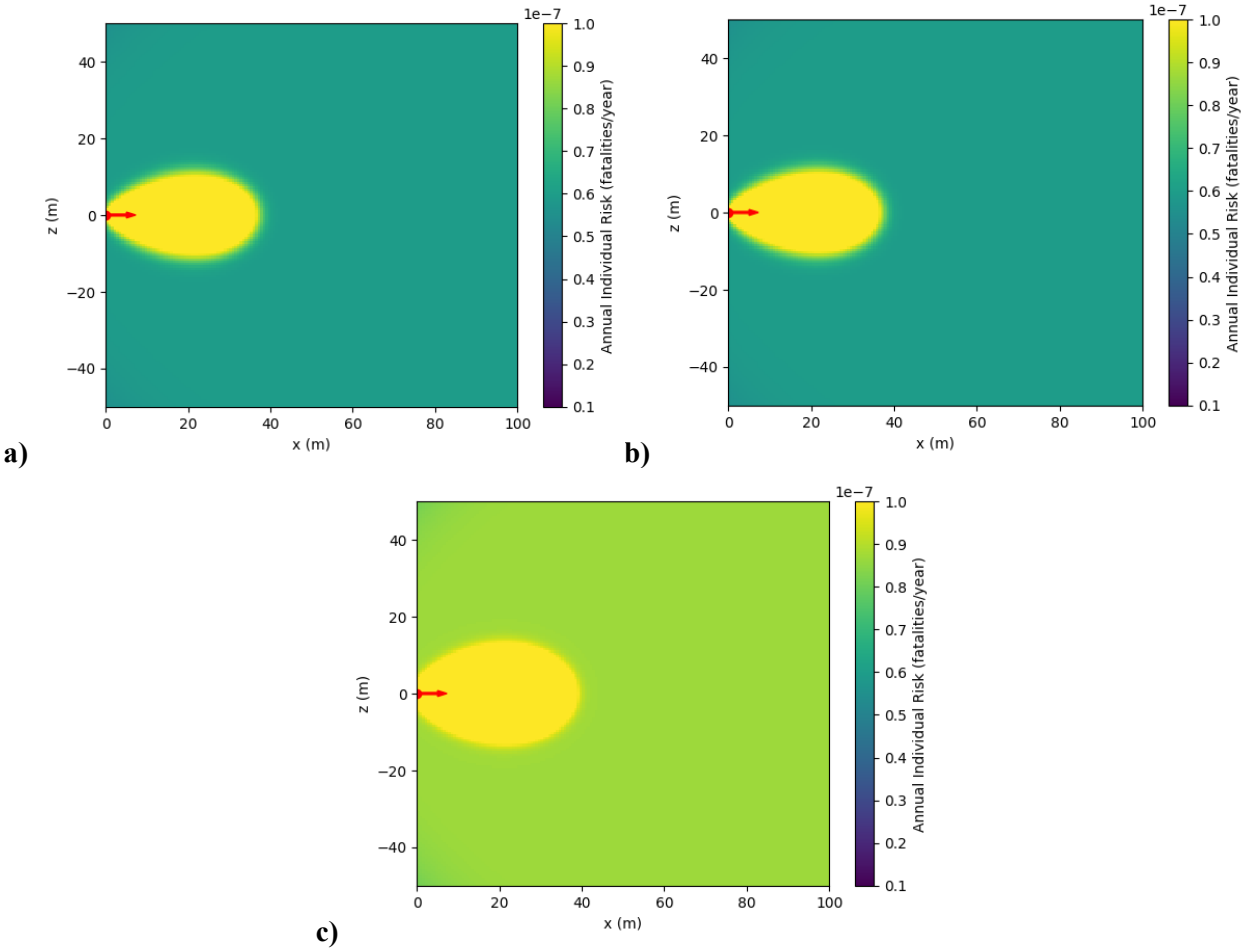


Figure 4-2. Annual individual risk for a person near an underground cavern wellhead (excluding processing facility) for configuration a) C1, b) C2, and c) C3.

Some countries such as the United Kingdom and Venezuela provide guidance for acceptable risk levels from different industrial activities, but the United States does not currently have a comparable risk acceptability standard. The United Kingdom Health and Safety Executive (U.K. HSE) is a well-regarded resource for risk-related guidance, especially in oil and gas operations and adjacent industries. In the absence of concrete national risk standards, the U.K. HSE can provide a frame of reference for risk results. For example, one recommendation for industrial plants suggests that the maximum tolerable individual risk for workers and the public should be 10^{-3} and 10^{-4} fatalities per year respectively [15]. The same document mentions that 10^{-6} is the broadly accepted individual risk for people in the vicinity of an industrial plant. From the results shown above, the maximum individual risk for each reservoir and cavern configuration is on the order of 10^{-7} fatalities per year, which, in this initial risk assessment of anticipated subsurface storage conditions for hydrogen, suggests that there is promise in designing hydrogen wells similarly to current natural gas wells without drastically increasing risk to operators and the general public in the vicinity. However, it should be noted that these example results are for a simplified example facility based on data from a single reference and based on a single set of input and parameter values, some of which may be highly uncertain; variability in site-specific designs and in the input/parameter values may change this risk value significantly.

As previously mentioned, Figure 4-1 and Figure 4-2 only show individual risk due to leaks from the wellhead. Figure 4-3 below shows the addition of the aboveground processing facility to individual risk from the R1 wellhead; results from the R2, R3, and cavern configurations are not shown because the processing facility risk is the same for all the wellhead configurations.

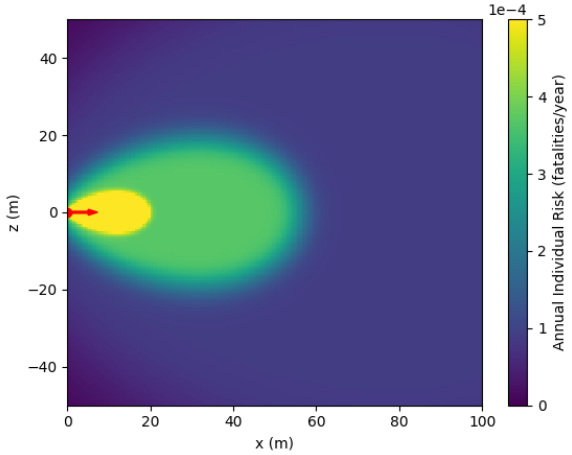


Figure 4-3. Annual individual risk for a person near the R1 wellhead and processing facility.

The risk contours in the graph above mimic the shape of heat flux contours from a jet flame; thermal effects from jet fires continue to dominate the overall risk while overpressure effects from explosions still do not show substantial contributions to risk. The graph contains distinct regions of risk, made obvious by the yellow, green, and blue colors. Each region corresponds to a heat flux profile from a different leak size. Heat flux contours are shown in Figure 4-4 for a jet fire from each leak size; the contour levels were selected as low (5 kW/m^2), medium (10 kW/m^2), and high (20 kW/m^2) heat flux thresholds and were taken from criteria used to determine liquid hydrogen setback distances for different exposure groups in the 2023 edition of NFPA 2 [8]. The lowest heat flux contour of 5 kW/m^2 is just above 4.732 kW/m^2, which "is defined by API 521 as the heat flux threshold in areas where emergency actions lasting several minutes might be required by personnel without shielding but with appropriate clothing" [8]. The highest heat flux contour of 20 kW/m^2 "is generally considered the minimum heat flux for the nonpiloted ignition of combustible materials, such as wood" [8]. The black line in the Figure 4-4 graphs shows the visible flame length of the jet fire. Juxtaposing Figure 4-3 and Figure 4-4, it is evident that the yellow contour in Figure 4-3 reaches around 20 meters in front of the leak and likely corresponds to the heat flux contour

for a 1% leak, shown in Figure 4-4(c). The green contour in Figure 4-3 reaches around 60 meters in front of the leak and likely corresponds to the Figure 4-4(d) heat flux contour for a 10% leak. The lighter blue contour that extends beyond the boundaries of the graph in Figure 4-3 likely corresponds to the heat flux contour from a 100% leak, shown in Figure 4-4(e). In Figure 4-3, the contours show elevated risk closest to the leak where the heat flux and risk contours overlap. The two smaller leak sizes (0.01% and 0.1% of the pipe area) are contained within the yellow contour of the Figure 4-3 plot but are not visible because of the scaling factor used on the color bar of the plot. Color bar scaling limitations are also responsible for the lack of visible discernment between risk levels from different leak sizes in the wellhead risk shown in Figure 4-1 and Figure 4-2.

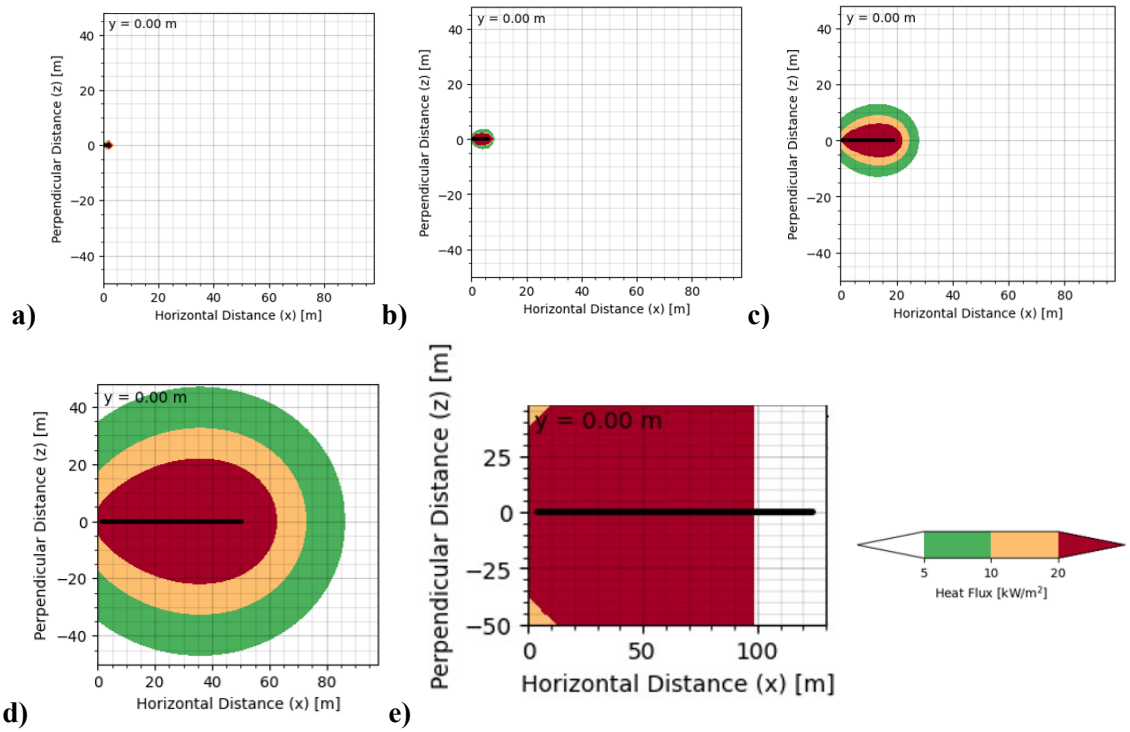


Figure 4-4. Heat flux contours for a jet flame from a leak that is a) 0.01%, b) 0.1%, c) 1%, d) 10%, and e) 100% of the pipe cross-sectional area (7-inch diameter pipe).

In Figure 4-3, the maximum calculated individual risk in this area is on the order of 10^{-3} fatalities per year; the overall risk is dominated by the processing facility. A comparison of the maximum calculated individual risk in this area of interest for each configuration and risk category is provided in Table 4-1 for reference.

Table 4-1. Maximum Individual Risk Results in Area of Interest

Well Configuration	Maximum Individual Risk from Processing Facility (fatalities/year)	Maximum Individual Risk from Wellhead Operations (fatalities/year)	Maximum Individual Risk from Wellhead Entry (fatalities/year)
R1	1.04×10^{-3}	1.32×10^{-7}	1.88×10^{-8}
R2	1.04×10^{-3}	1.32×10^{-7}	6.95×10^{-8}
R3	1.04×10^{-3}	1.23×10^{-12}	11.1×10^{-8}
C1	1.04×10^{-3}	1.32×10^{-7}	1.88×10^{-8}
C2	1.04×10^{-3}	1.32×10^{-7}	1.88×10^{-8}
C3	1.04×10^{-3}	1.32×10^{-7}	7.18×10^{-8}

The maximum individual risk from the processing facility is located within 20 m of the leak in the x-direction (directly in front of the leak), so it is more relevant to facility operators than to the public. As a comparison to the U.K. HSE acceptable risk guidelines, this processing facility risk is nearly the same as the maximum tolerable individual risk for workers, and orders of magnitude higher than the broadly accepted 10^{-6} probability of fatality metric. Additionally, there is an area between around 20 and 60 meters in front of the leak where the individual risk is between $3–5\times10^{-4}$ fatalities per year. This is on the same order of magnitude as the maximum tolerable individual risk for the public and several orders of magnitude higher than 10^{-6} fatalities per year. Thus, this analysis suggests that the processing facility should be an area of focus when implementing safeguards into the system design. The consequences (i.e., probabilities of fatality) from the wellhead and processing facility are similar because they have similar leak sizes, with a maximum leak size of 180 mm, so the leak frequencies rather than the consequences are likely the cause of their differences in risk. Based on the leak frequency data used in this study, the filters, instruments, and compressors in the processing facility have especially high leak frequencies, even for large, high consequence leak sizes. Therefore, this study indicates that particular action to prevent leaks in these components would be most effective in reducing individual risk from the processing facility. Measures such as frequent maintenance, repair and replacement of these components are examples of ways to mitigate this risk. However, it should also be noted that the HyRAM+ default leak frequencies and the wellhead leak frequencies were derived and reported from generic leak data with few and no hydrogen-specific data points. It is possible that the true hydrogen leak frequencies that would be expected from this type of facility are different from those estimated in HyRAM+ or reported in [5]. Improving the state of knowledge on leak frequencies for hydrogen systems could therefore change the conclusion that the processing facility would contribute more to overall risk than the wellhead.

4.2 Societal Risk Results

As described in Section 0, the societal risk results were evaluated in terms of F-N curves. These results are shown in Figure 4-5 for the depleted hydrocarbon reservoir configurations and Figure 4-6 for the cavern configurations. Tabulated results for the F-N curves are provided in Appendix E.1.

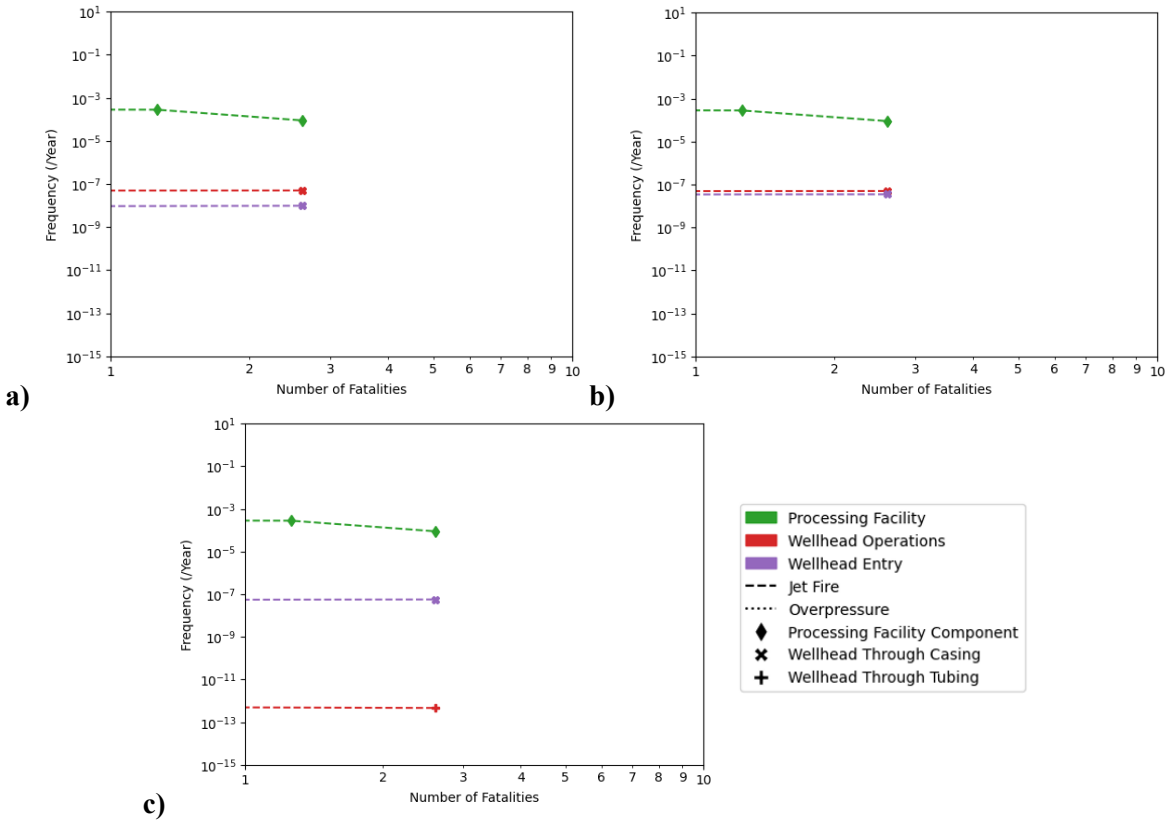


Figure 4-5. F-N curves showing societal risk for the area of interest with a population density of 2700 people per square mile for a) R1, b) R2, and c) R3.

These plots were truncated to show physically meaningful numbers of fatalities greater than one; only the F-N points from the largest leak sizes can be seen. The colors on the plots discern between the origin of the leak (the processing facility or the wellhead during regular operations or maintenance entry). The same processing facility assumptions were used for each configuration, and the processing facility risk leak frequencies are the highest compared to the wellhead leak frequencies, for all configurations. For configurations R1 and R2, the leaks during normal wellhead operations are the next most frequent while leaks from wellhead entry are least frequent. For configuration R3, the wellhead entry leaks are more frequent than leaks during normal wellhead operations. One reason for there being less frequent leakage during normal operations in configuration R3 is the increased amount of equipment used to prevent unintended fluid flow, such as the packer and DHSV. The greater number of components also introduces complexity into the system that may warrant more frequent wellhead entries in R3 compared to R1 and R2, causing the R3 wellhead entry leaks to also be more frequent. Table B-9 shows the higher number of annual entries into the R3 wellhead.

The shapes of the markers on the plot differentiate between leaks in specific wellhead components and pathways – leaks through the casing, leaks through the casing and wellhead, and leaks through the tubing and wellhead. This example study only revealed a slightly lower annual number of leaks from the wellhead through tubing pathway than from the other two pathways. However, as mentioned previously, the leak pathways were assumed since they were not explicitly provided in [5]. In general, this type of analysis can be used on specific systems to determine which leak pathways are the most vulnerable so they can be the focus of leak mitigation efforts. Again, the availability of more hydrogen-specific leak frequency data would lead to higher confidence in conclusions made about leak pathways of concern, so this type of risk assessment may become more robust as hydrogen systems are more widely deployed and better understood.

The line styles in Figure 4-5 show a comparison between risk from a jet fire and from an explosion. The plots were truncated to show numbers of fatalities greater than one; the calculated overpressure response was low enough that the expected number of fatalities was below one for both the wellhead and the processing facility; thus, the overpressure lines are not seen on the graph. The low consequence of an overpressure event in this system is likely from the assumed flame speed of Mach 0.35, which was used to represent a low degree of obstructions present near the storage facility. The facility would be built to reduce the number of obstructions according to NFPA 2 [8], to limit the creation of confined spaces in which a leaked flammable gas cloud could accumulate, gain turbulence, and ignite into deadlier explosions. Furthermore, the facility would already be outdoors, minimizing the number of structures nearby that could contribute to flammable gas accumulation. The subsonic Mach flame speed represents a scenario in which the hydrogen is most likely to dissipate before generating an explosion as deadly as the jet fires from the same leak sizes. Overpressure risk for operational failures in wellhead R3 is not even visible in the graph because a low fatality number was calculated from overpressure effects.

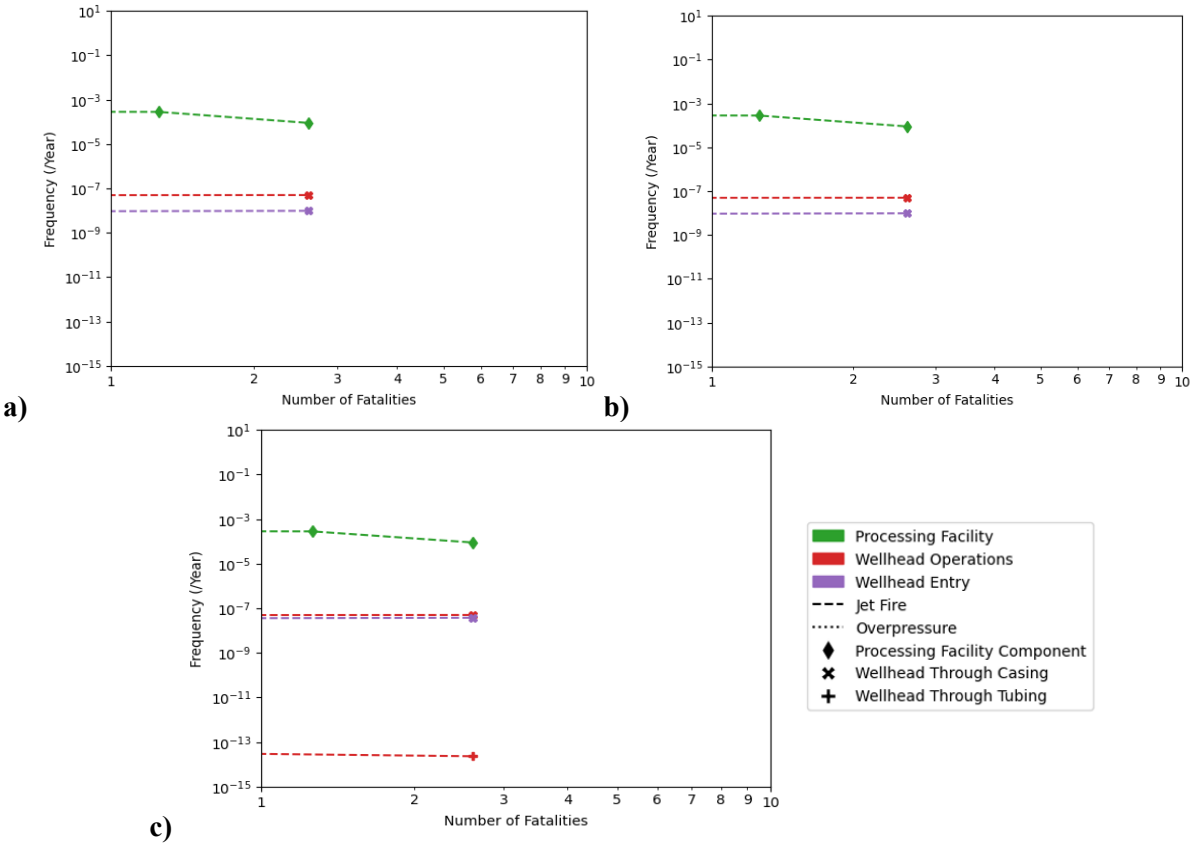


Figure 4-6. F-N curves showing societal risk for the area of interest with a population density of 2700 people per square mile for a) C1, b) C2, and c) C3.

Many of the same observations from Figure 4-5 apply to Figure 4-6. The processing facility still has the highest leak frequencies compared to wellhead both during normal operations and during maintenance entry. Unlike components like the DHSV in the reservoir configuration, which is explicitly considered a safety feature to prevent leaks, the added casings in cavern configurations C1 to C3 are not specifically used to prevent a kick (unintended flow of stored fluid from the well to the wellbore) or a blowout. However, the additional intermediate casing and tubing in C3 still add extra components through which stored gas must travel to leak to the outside of the wellhead, which leads to the lower operational leak frequencies in the C3 wellhead compared to the C1 and C2 wellheads. Like in the reservoir configurations with more components, C3 also shows higher frequencies of adverse events from leaks during wellhead

entries since it undergoes more entries each year, possibly because of the more complex design. Figure 4-6(c) also shows that leaks from the wellhead through the tubing happen least frequently and leaks from the wellhead through the casing happen the most frequently out of the three external leak points, but, again, this analysis should be used as an example of how leak points in a more specific system can be compared rather than to conclude that the wellhead through casing leak pathway should be the focus of all wellhead leak mitigation plans.

When comparing the reservoir and cavern configurations in general, the wellhead operational risk tends to be similar, with adverse events from leaks occurring between 10^{-14} and 10^{-10} times per year. The slight differences in well entry risk are largely dependent on the number of well entries that happen each year.

4.3 Sensitivity Study

The following sensitivity studies were conducted for the R1 reservoir configuration; however, as discussed in Section 4.1, the processing facility dominates the individual risk in comparison to the wellhead operations and wellhead entry, so the sensitivity results would be similar for all the wells described in this report since the same processing facility is used for all configurations.

The results for the sensitivity study are tabulated in Appendix E.2.

4.3.1 Mach Flame Speed

The contours in Figure 4-7 show a comparison between individual risk when the leaking hydrogen plume has a flame speed of Mach 0.35 and Mach 5.2.

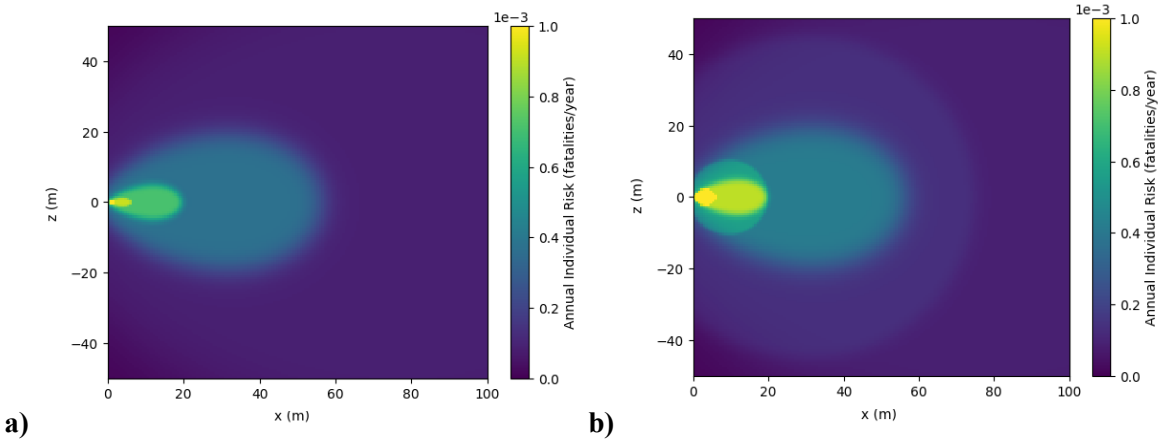


Figure 4-7. a) Individual risk contour for flame speeds of a) Mach 0.35 (default) and b) Mach 5.2.

The contour plot representing the case with a flame speed of Mach 0.35 shows an individual risk contour whose shape predominantly emulates that of a jet flame, where the greatest risk occurs along the line of the jet flame in the x-direction and tapers off in petal-like contours. The contour plot for the case with a flame speed of Mach 5.2 shows an obvious addition to the risk from overpressure effects – while the jet flame shape is still present, there is also evidence of an overpressure contribution that has an origin some distance in front of the leak and emanates radially outward. This leads to an increase in overall risk in some places, especially close to the leak.

A contour plot showing the increase in risk at each location from the increased flame speed is provided in Figure 4-8. This explicitly shows the contributions of overpressure to the overall risk, with clear circular

risk contours. The overpressure from a plume flame speed of Mach 5.2 increases individual risk within an order of magnitude of 10^{-4} fatalities per year for locations within around 80 meters in the x-direction and 40 meters in either z-direction of the leak, which is not insubstantial considering the individual risk with a plume flame speed of Mach 0.35 was also on the order of 10^{-4} fatalities per year.

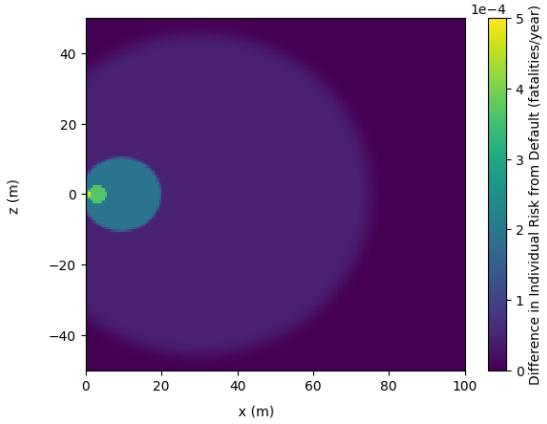


Figure 4-8. Contour showing difference in individual risk with flame speeds of Mach 5.2 and 0.35.

There are four visible contours in Figure 4-8. Each one represents the additional overpressure risk from a different leak size in the processing facility (although the wellhead risk may also increase from a higher Mach flame speed, the risk is still dominated by the processing facility). There are five leak sizes considered in the processing facility, but only four contours are visible on the plot for the four smallest leak sizes, since the largest leak size leads to an increased plot contour that is beyond the boundaries of the graph. Larger leaks have overpressure origins that are slightly farther from the leak in the x-direction and elevated overpressure contours with larger radii because there is a higher mass flow rate of hydrogen exiting the leak and a larger flammable mass available for delayed ignition. The contours in Figure 4-8 show larger increases from the Mach 0.35 flame speed case to the Mach 5.2 flame speed case closer to the leak because there are more overlapping overpressure contours close to the leak from larger leak sizes. Overpressure contours for an explosion from each leak size and each Mach flame speed are shown in Figure D-11 for context.

One additional way to compare the individual risk using two different Mach flame speeds is by using a line plot; however, the line plot is one-dimensional in terms of the number of spatial directions it can portray. Figure 4-9 shows a line plot of individual risk for each scenario at different distances along the leak (directly in front of the leak point, at 0 meters in the z-direction), which provides an idea of the variation in risk even though the graph would look slightly different if the z-coordinate were to be shifted. Like the contour plots, the line plot shows that most points between 0 and 80 meters in the x-direction in front of the leak experience a difference within around 10^{-4} fatalities per year of risk when the Mach flame speed of the plume is varied from 0.35 to 5.2. The increased overpressure does not have a noticeable influence outside of that 80-meter range.

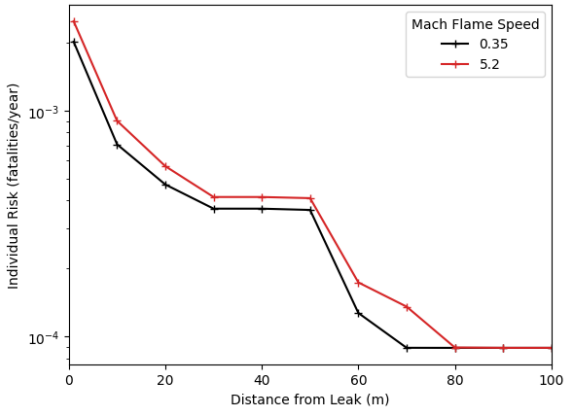


Figure 4-9. Individual risk directly in front of leak for default (0.35) and higher (5.2) Mach flame speed.

This type of sensitivity study can broadly be used to anticipate higher risk in certain wellhead and processing facility designs. For example, a facility that is set up with any sort of enclosure around the wellhead or processing equipment would likely lead to higher risk from potential overpressure events, both for people working at the facility and for those who reside or work outside of it. This type of sensitivity study can be informative to wellhead owner-operators, who may choose to design their wellhead without an enclosure or any walls such as fire barriers nearby; if a facility enclosure is necessary for other reasons such as weather or security, they may increase setback distances to exposures like other equipment and people outside of the facility. There is also currently limited guidance in safety codes and standards for UHS system design, so this type of sensitivity study can also inform new regulations that may emerge to serve this application. For instance, regulatory bodies may choose to limit the degree of confinement or enclosures allowed in UHS systems or may issue different setback distance requirements for facilities that do have some degree of confinement in their design.

4.3.2 Ambient Conditions

The next sensitivity study focused on different ambient conditions that might be present around a UHS site at any time of year. Figure 4-10 below shows contour plots comparing individual risk from the default HyRAM+ ambient conditions and conditions from a higher temperature and lower humidity case. Although this was only one combination out of several temperature-humidity cases, only one contour is included as an example because the contour plots all looked fairly similar.

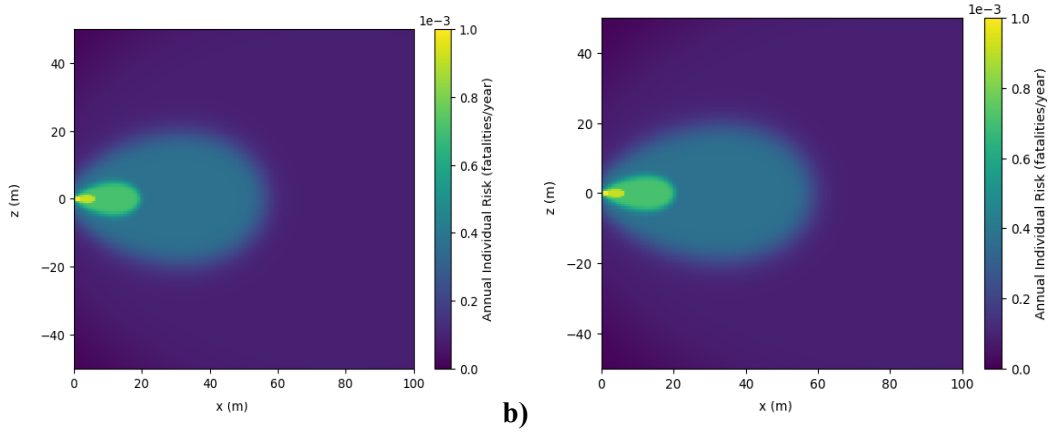


Figure 4-10. Individual risk contour using a) default ambient conditions (20°C and 89% humidity), b) example ambient conditions for summer in Beaumont, TX (44°C and 52% humidity).

As previously mentioned, the differences in individual risk are difficult to discern based on the risk contours shown above since the differences likely happen on a lower order of magnitude than the scale of the color bar. Therefore, Figure 4-11 shows a contour plot with the difference between the individual risk from each scenario and from the default ambient conditions.

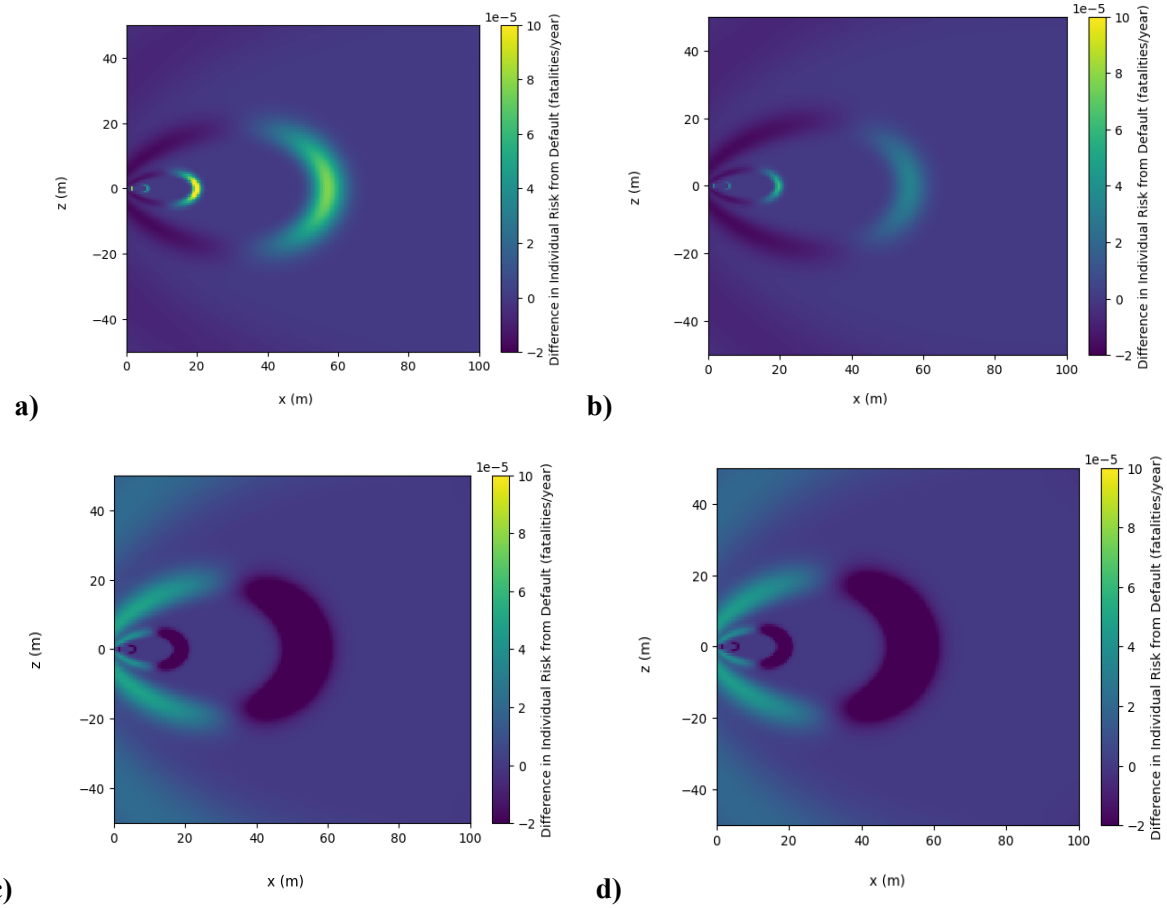


Figure 4-11. Contours showing difference in individual risk between default ambient conditions (20°C and 89% humidity) and a) Beaumont, TX summertime case (44°C and 52% humidity), b) Charleston, SC summertime case (32°C and 90% humidity), c) St. Clair, MI wintertime case (-18°C and 60% humidity), and d) Allegany, NY wintertime case (-19°C and 89% humidity).

The two contours on the top show a high temperature case, the two contours on the bottom show a low temperature case, the two contours on the left show a low humidity case, and the two contours on the right show a high humidity case. The top two graphs representing an elevated temperature show lower risk values offset in the z-direction close to the leak and higher risk values straight in front of the leak in the x-direction. The bottom two graphs representing a lower temperature show the opposite trend, with higher risk values offset in the z-direction close to the leak and lower risk values straight in front of the leak in the x-direction, for each leak size visible on the graph. These trends can be explained by analyzing the heat flux contours in each ambient condition scenario. The higher ambient temperatures lead to flames that emit a heat flux profile that is longer in the x-direction and thinner in the z-direction close to the leak than the heat flux profiles with the default ambient temperature, likely because the air viscosity decreases at a higher temperature, allowing for the momentum-driven jet to travel farther. Likewise, the lower ambient temperatures lead to flames that emit a heat flux profile that is shorter in the x-direction and wider in the z-direction close to the leak than the heat flux profiles with the default ambient temperature. Effects of ambient humidity are less noticeable; the two bottom graphs in Figure 4-11 show scenarios

with very similar ambient temperatures and different humidities and the variation in risk that these humidities lead to is imperceptible compared to the effects of ambient temperature on risk. The heat flux contours for each leak size and ambient condition scenario are provided for reference in Figure D-12, Figure D-13, Figure D-14, Figure D-15, and Figure D-16.

The line plot below shows the individual risk along the leak, at various points in the x-direction when z=0 meters. The change in risk between different cases within around 70 meters of the leak is within an order of magnitude of 10^{-4} fatalities per year. At points where the risk seems to differ between cases, the high-temperature ("summer") cases show slightly elevated risk while the low-temperature ("winter") cases show slightly decreased risk from the default ambient conditions. The temperature seems to have a greater impact on risk than humidity, since the two low-temperature cases have nearly the same ambient temperature and around a 30% difference in humidity but an imperceptible difference in risk in this line plot.

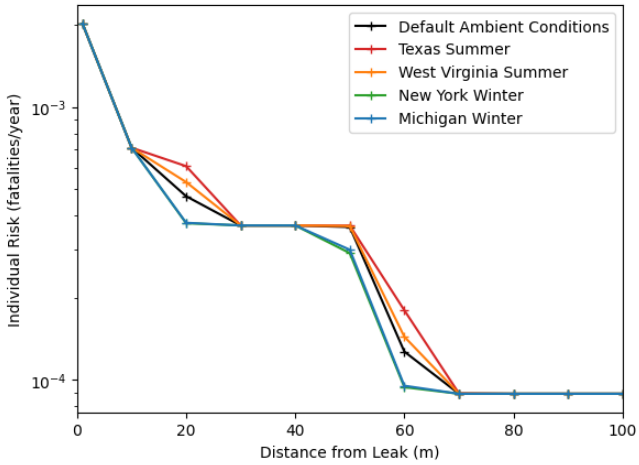


Figure 4-12. Individual risk directly in front of leak for different ambient conditions.

Like the Mach flame speed sensitivity study, this ambient condition sensitivity study can also broadly inform UHS stakeholders like wellhead owner-operators and safety codes and standards committees on how to design low-risk systems. This analysis revealed different ambient conditions that could lead to somewhat higher risk in different locations; for instance, higher ambient temperatures led to longer flames. Thus, it is possible that stakeholders would want wellhead designs to account for the more conservative case of higher temperature extremes by implementing longer setback distances. This is a general example of how this type of sensitivity study can provide justification for design and regulatory decisions, but, in practice, those decisions would also incorporate more considerations including aspects like acceptable risk, overpressure and heat flux thresholds, and permitting and land use regulations. This example also illustrates how conditions that can change day-to-day (or even hour-to-hour) at a given location can affect the risk outcome, emphasizing how variable these types of calculations are and how important it is to consider the range of possible conditions.

4.3.3 Underground Storage Conditions

Changing the underground storage conditions from 30 MPa and 80°C (149°F) to 40 MPa and 65°C (176°F) led to a negligible change in individual risk, so these plots are not included. The reservoir or cavern pressure and temperature can both deviate from either of these conditions depending on factors like the geological attributes and depth of the well. However, only pressures on the upper end of the ranges discussed were tested in this sensitivity study because higher pressure storage conditions for hydrogen are more efficacious for storing meaningful and useful quantities of hydrogen.

4.4 Temporal Leak Analysis

The following figure shows the drawdown of an underground hydrogen storage well in terms of wellhead pressure over time, for three different leak sizes.

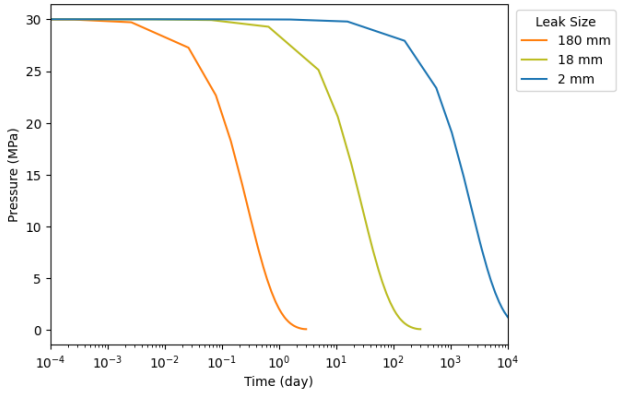


Figure 4-13. Wellhead pressure for the full duration of a blowout.

Pressure in an underground storage well must be maintained during normal operation for it to properly manage gas injections and withdrawals. The depletion of a well and corresponding pressure drop over the course of a blowout can provide some indication of how much product must be replenished for the well to return to operating condition (disregarding other damage to equipment and infrastructure that may have occurred during the blowout). Figure 4-13 shows that when the well has a large leak, it sustains normal operational wellhead pressure for around 10 minutes before decreasing more rapidly. In the case of such a large leak, there is a low likelihood that a repair would be attempted at all, much less within the first 10 minutes, because of the high risk and low probability of a successful intervention. Thus, starting up the well again after a large leak would likely require replenishing the entire well with hydrogen. The medium leak sustains pressure for around 16 hours before losing pressure more rapidly. Comparing this case to the 111-day Aliso Canyon leak, this underground well would have been depleted to less than 5 MPa of pressure with a medium-sized leak, in which case the well pressure would still need to be replenished significantly for the well to return to normal operations. The small leak sustains around 30 MPa of pressure for about 70 days before beginning to decrease in pressure more rapidly. A small leak would be less damaging and dangerous to manage than a larger leak, so it is possible that the leak could be discovered and repaired before causing significant pressure depletion of the well. However, it may also be more difficult to detect a small leak, especially in the absence of a noticeable pressure drop in the well, so the leak detection equipment around the wellhead should be considered when designing a wellhead for an underground hydrogen storage reservoir or cavern. It should be noted that the time axis of the figure is logarithmic, and the pressure decrease in the wellhead due to the small leak happens at a much slower rate than the pressure decreases from the larger leaks.

Table 4-2 shows the duration of a complete well drawdown using each leak size. One simplification to consider here is that only 900,000 m^3 of hydrogen was considered to be present in the well. In many oil and gas fields, the subsurface material is porous, and wells may be connected to each other in a way that allows gas to easily travel between wells. This detail was not included in the analysis for simplicity.

Table 4-2. Complete Drawdown Time by Leak Size

Leak Size (mm)	Time for Complete Drawdown
180	36 hours
18	150 days (~5 months)
2	66 years

The largest leak size, also classified as a rupture in [5], leads to a 36-hour blowout. Generically based on the large orifice size and the high probability of ignition, it is likely a leak of this size would be left to draw down the well because of the difficulty of quickly killing the well with such a large leak and the danger of jet fires or explosions from the leaking gas. The 180-mm rupture is similar in size to the Aliso Canyon leak, which was caused by the rupture of a 7-inch (178 mm) pipe [16]. The 18-mm leak size included in this report would lead to complete drawdown over 150 days, which, depending on conditions, could be enough time to stop the leak before complete depletion of hydrogen from the well. The smallest leak size would take so long to completely draw down the well that it would likely be detected and repaired before any consequential depletion of the well occurred.

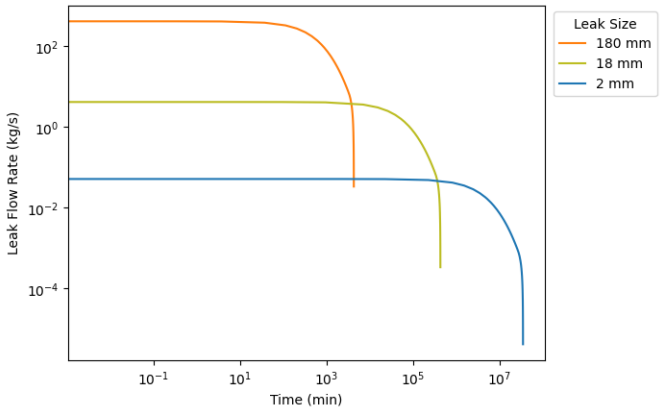


Figure 4-14. Release rate of hydrogen from leak for the full duration of a blowout.

The release rate of hydrogen from the leak over time is indicative of how likely the hydrogen is to ignite. The 180 mm leak releases around 419 kg/s of hydrogen during the steady-state portion of the leak, which corresponds with a 23% probability of a jet fire and 12% probability of an explosion (see Table A-1). The 18 mm leak releases around 4.19 kg/s of hydrogen during its steady state, which corresponds with a 5.3% probability of a jet fire and a 2.7% probability of an explosion. The 2 mm leak releases around 0.05 kg/s of hydrogen during its steady state, leading to a 0.8% probability of a jet fire and a 0.4% probability of an explosion. The ignition probabilities are one indication of how likely a leak of each size can cause damage to surrounding equipment and infrastructure. However, it should be noted that these ignition probabilities come from a single source [17] that acknowledges a high degree of uncertainty; while it seems physically plausible that a high-flowrate leak is more likely to ignite than a low-flowrate leak, the actual value of this probability is not well known. The ignition probabilities used in this report are provided in Appendix B.1.

In the case that the leak ignites immediately, resulting in a jet fire, both the duration and reach of the effects of the jet fire are important for determining the potential damage to nearby stationary equipment and infrastructure. Figure 4-15 shows the visible flame length of the jet flame from each leak size.

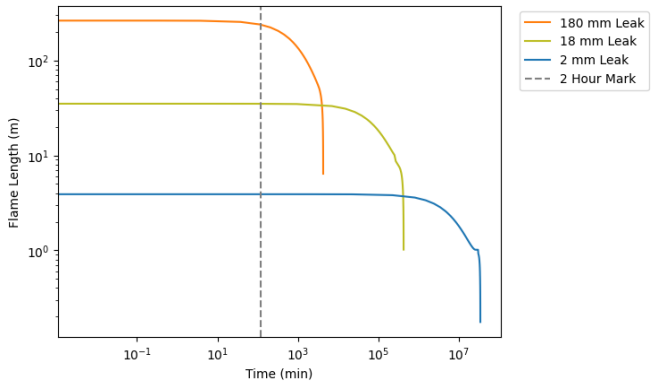


Figure 4-15. Jet fire visible flame length for the full duration of a blowout.

The steady-state flame lengths differ drastically between the orifice sizes considered; the jet flame from the smallest leak is under 10 meters long, the jet flame from the medium leak is between 30 and 40 meters long, and the jet flame from the largest leak is between 200 and 300 meters long. The two-hour time is shown just as a reference since many fire protection standards such as some NFPA codes contain requirements for the inclusion of two-hour rated fire protection walls.

Another way to understand the potential damage of a jet fire over time is by tracking the level of radiative heat flux over time. Contours showing a cross-section of the center of the flame from the side are shown in Figure 4-16 (the z-direction describes the horizontal offset from the flame path). Like the jet fire flame length in Figure 4-15, these contours show that the most harmful heat fluxes reach under 10 meters for the smallest leak, on the order of tens of meters for the mid-sized leak, and on the order of hundreds of meters for the largest leak.

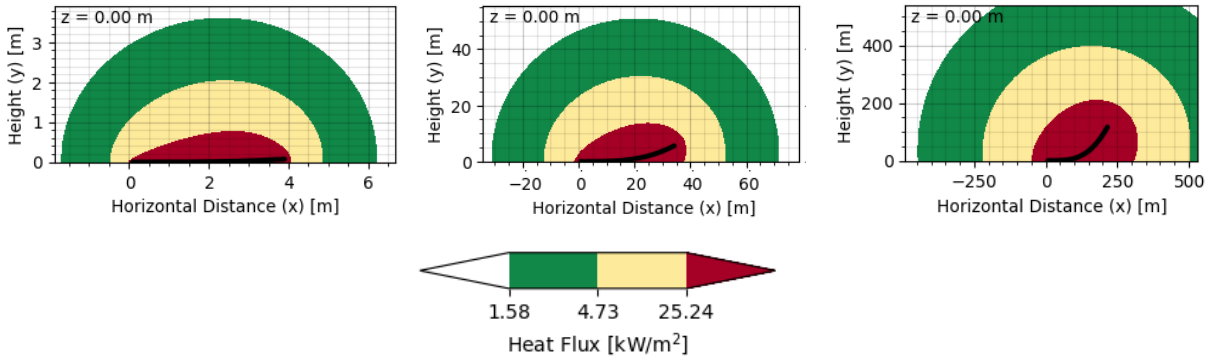


Figure 4-16. Heat flux contours for the steady-state jet fire from a 2 mm (left), 18 mm (middle), and 180 mm (right) diameter leak. Heat flux levels are taken from HyRAM+ default levels.

Certain levels of heat fluxes at prolonged times can lead to different types of damage to infrastructure. LaChance et al. provides examples of heat flux levels and exposure times that lead to certain general damage outcomes in infrastructure [18].

Table 4-3. Damage to Structures and Equipment from Thermal Radiation, taken from [18].

Thermal Radiation Intensity (kW/m^2)	Exposure Time (min)	Type of Damage
4	30	Glass breakage
12.5-15	>30	Piloted ignition of wood, melting of plastics
18-20	>30	Cable insulation degrades
25-32	>30	Unpiloted ignition of wood, steel deformation
35-37.5	>30	Process equipment and structural damage (including storage tanks)
100	>30	Steel structure collapse

The duration time for the building damage metrics in [18] is 30 minutes, and Figure 4-15 shows that the steady-state flame occurs for longer than 30 minutes for all three leak sizes. These heat fluxes are tabulated by distance in front of the leak in the Table 4-4 heat map.

Table 4-4. 30-Minute Heat Fluxes Over Distance for Each Leak Size.

Leak Size (mm)	Approximate 30-Minute Heat Flux (kW/m^2) at X Distance from Leak									
	10 m	20 m	30 m	40 m	50 m	60 m	70 m	80 m	90 m	100 m
2	0.4	0.1	0	0	0	0	0	0	0	0
18	4,830	700	130	17	6	3	2	1	1	1
180	605	1790	3300	5940	11,440	6700	3310	2130	1610	1080

Heat Map Legend
< 4 kW/m^2 Causes no discernible damage over 30 minutes
4-20 kW/m^2 May cause glass breakage, piloted ignition of wood, melting of plastics, degradation of cable insulation over 30 minutes
>100 kW/m^2 May cause unpiloted ignition of wood, deformation of steel, damage to process equipment and structures, collapse of steel structures over 30 minutes

According to these metrics, within 30 minutes, a small leak jet fire impinging on any structures between 10 and 100 meters away would not cause significant damage. The medium leak jet fire would cause significant damage to structures within 30 meters, moderate damage to structures between 40 and 60 meters, and minimal damage to structures beyond 60 meters away. The largest leak would create a jet fire that would damage structures over 100 meters away; the steady-state radiative heat flux from this large jet fire takes around 200 meters to reach below 100 kW/m^2 and reaches below 10 kW/m^2 over 350 meters away from the leak. This calculation is conservative in that it assumes the flame is directly horizontal and impinging on a structure, and that there is no wind to dilute the concentration of hydrogen to below the flammability limits. It also uses a narrow set of time metrics to determine damage levels. Figure 4-15 shows that all three flames are sustained for longer than 30 minutes, which could potentially cause greater damage than the levels indicated in [18]. Despite these limitations in available heat flux damage metrics, Table 4-4 provides a general indication of which buildings may be vulnerable to wellhead jet fires, and the extent of the damage that may occur. While a jet fire from a small leak may pose minimal threat to the

equipment and infrastructure both within and beyond the hydrogen storage facility, the jet fire from the medium-sized leak may cause significant damage to infrastructure within the facility or to unrelated structures located within 40 meters of the facility, and moderate damage to unrelated structures within 40-60 meters of the facility. A jet fire from the largest leak could have catastrophic implications for structures even hundreds of meters outside of the facility.

Other potential effects from long-term releases from a wellhead should also be considered. For example, the months-long methane leak from Aliso Canyon led to adverse health effects for members of the nearby community, including impaired cognition and respiratory function [19]. Few, if any, health studies are available regarding the community health effects of long-term respiration or exposure to elevated concentrations of hydrogen. One clinical study on healthy adults by Cole et al. revealed no adverse pulmonary, neurological, hematological, or cardiovascular effects from prolonged inhalation exposure to 2.4% hydrogen [20], which is one indication that leaking hydrogen would affect the health of the surrounding community much less than leaking methane, if at all. Additionally, the low density and small molecular size of hydrogen in comparison to methane means that hydrogen would be less likely to remain at ground level for meaningful amounts of time. If methane or another gas other than hydrogen were used as a cushion gas for the well, health effects from air quality may be more of a concern.

This temporal leak analysis highlights some important differences in assessing the risk of an aboveground hydrogen leak from a UHS wellhead and a facility that stores the hydrogen in aboveground tanks. Some aspects of the risk assessment from these two types of facilities would be the same, such as the processing equipment (e.g., compressors, filters). However, the UHS hydrogen storage could all be stored in a single well, meaning that if a leak were to occur from the wellhead, it could release the entire storage quantity if stopping it were not possible. By contrast, gaseous hydrogen stored in aboveground tanks are likely to utilize multiple smaller tanks, which are more practical to manufacture. If a leak were to occur in a hydrogen storage tank, the entire quantity of that tank could be released without releasing the hydrogen from the nearby tanks. It is possible, however, that a leak from one tank damages and causes a leak in a nearby tank, so even for aboveground tanks it is possible that a single leak may end up causing the release of the entire storage quantity. Larger aboveground tanks may be developed or used in the future, and multiple smaller-capacity wells in the same facility means that the exact storage configuration is facility-specific. It is always important to consider that the leak size and storage quantity can both affect the leak duration and outcomes, and that both can be scenario- and design-specific.

5.0 Conclusion

This report shows several example risk assessment methods and metrics that can be used to evaluate, inform, and develop regulations for safe UHS system design. The UHS system analyzed in this report consisted of a wellhead and an aboveground processing facility. The two types of underground geological formations that are currently used for subsurface natural gas storage are depleted hydrocarbon reservoirs and salt caverns; three configurations of each type of formation were considered in this analysis for use with UHS. The focus of the risk assessment was the hazards of leaks occurring in which hydrogen would be unintentionally released from within the system to the ambient air.

HyRAM+ QRA methods were used to calculate individual risk from steady-state leaks occurring from the wellhead, either during normal operations or during routine well entry, and from the aboveground processing facility during normal operations. These individual risk contours revealed that thermal risk from leaks that immediately ignite into jet fires dominates the risk compared to the overpressure risk from leaks that ignite after a delay and explode. This result is most likely attributed to the low Mach flame speed due to the assumption of all the equipment being outside instead of enclosed. This finding may be informative to stakeholders to focus more on risk mitigation actions targeting fire, such as implementing fire barrier walls where helpful and developing a specific and rigorous fire response protocol. The individual risk analysis also revealed that, based on the leak frequency data available, the risk from the processing facility was many orders of magnitude greater than the risk from the wellhead. The assessment in this report suggests that it may be beneficial for design and operation protocols to prioritize risk mitigation in the processing facility, though more hydrogen-specific leak frequency data is needed to have confidence in this conclusion. The individual risk assessment also showed that the configuration of the wellhead did have some impact on risk; specifically, the R2 reservoir configuration and the C3 cavern configuration had slightly elevated risk results compared to the other configurations. However, the differences in risk between configurations were many orders of magnitude smaller than the differences between the wellhead and the processing facility. This type of result can be helpful because selecting a wellhead configuration may not always be possible in the presence of other challenges such as economic and design considerations for specific geologic formations.

Examples of societal risk calculations were also shown, to consider people outside of and unaffiliated with the facility who might still be within reach of the harmful effects of a leak at the facility. This analysis showed the risk in terms of the number of expected fatalities as a percentage of the population in a chosen area of interest, and the annual frequency of each type of harmful effect (jet fires and explosions). The results were parsed out by the part of the facility (wellhead vs. processing facility) and the leaking component in the wellhead (a leak through the casing vs. through the tubing). The processing facility showed much higher frequencies of leaks and therefore jet fires and explosions than the wellhead; for most of the configurations, the wellhead operations and wellhead entries led to similar frequencies of these effects. Within the wellhead, leaks in the wellhead through the casing appeared to occur with higher frequency than leaks in the wellhead through the tubing, which would in this case indicate that leak prevention and detection efforts should prioritize where the wellhead and casing meet. In terms of number of expected fatalities, the largest leaks among the processing facility, wellhead operations, and wellhead entry leaks led to the maximum number of fatalities in the area of interest. The same societal risk analysis was also presented in terms of the number of people expected to reside within that area of interest based on a county population density from a database of the locations of existing UNGSFs in the United States. The low population densities considered reflect how many of the existing UNGSFs are located in remote areas. However, this was an imperfect way to depict population in the area of interest because the length scale of leak effects is on the order of tens of meters while county populations can span areas with much larger length scales; it is inaccurate to downscale this geospatially averaged population density number because within the 50 m x 50 m area of interest there could be regions with higher or lower

concentrations of people. The analysis also used the assumption that the people in the area of interest are always present in that area when in reality they would likely move in and out of the area throughout each day and throughout the year. Therefore, societal risk calculations for specific UHS systems should be customized by location and the habits of people nearby. For example, using neighborhood populations would be a much more accurate way to consider the population that would be potentially affected by the UHS facility.

A sensitivity study was used to understand the effects of different inputs or assumptions on individual risk. Increasing the Mach flame speed, which physically represents a wellhead or processing facility design with more walls or confined spaces, led to an increase in individual risk from overpressure. Increasing the ambient temperature led to a flame and thermal risk contour with a longer reach directly in front of the leak and a slightly shorter reach out to the side close to the leak point. Decreasing the ambient temperature led to a flame and thermal risk contour with a shorter reach directly in front of the leak and a slightly longer reach out to the side close to the leak point. The impact of relative humidity on individual risk was imperceptible. These types of sensitivity studies can be used to inform safe well design as well as the broader regulatory landscape of UHS.

Finally, a temporal leak analysis was used to evaluate the potential extent and reach of damage from a jet fire over the course of a leak. This type of analysis was used to complement the steady-state risk analyses to capture how the extent of damage from a jet fire, especially to infrastructure within the facility and nearby, can change over time. The well pressure over the course of the drawdown of a well can be helpful as an indication of how much product has been lost over time, and how unstable the well formation may be as a result of pressure loss from a leak. The flame length over time shows the potential reach of a flame from a leak, which can inform setback distances or provide information about where to place protective infrastructure like fire barrier walls. Heat flux contours over time can show both the extent of damage (based on levels of heat flux) and reach of damage (based on the distance reached by those harmful levels of heat flux). These results were shown for three different leak sizes. As discussed in the body of the report, smaller leaks would have smaller consequences, including shorter jet flames and lower heat fluxes farther from the leak, in addition to being easier than larger leaks to stop and repair. Larger leaks and ruptures lead to worse consequences like longer jet flames and higher heat fluxes farther from the leak, which means they could potentially affect more people and damage more buildings, especially those that are outside of the facility. These types of leaks have historically been dangerous and logistically difficult to stop in the oil and gas industry. However, hydrogen has different properties and behaviors than natural gas, so more research should be conducted to understand how to kill UHS wells during large leaks or blowouts, and the associated hazards of UHS blowouts. There are also other temporal effects of a leak that could be of concern besides jet fires, such as air quality. This issue was not addressed extensively in this report besides general predictions that hydrogen contamination in the air would not be as harmful on human health as fuels like natural gas, based on small-scale studies of elevated levels of hydrogen in air. Air quality is another area that should be researched in more detail as UHS technology and deployment continues to develop.

6.0 References

[1] "SHASTA Brochure." [Online]. Available: https://edx.netl.doe.gov/shasta/

[2] "Natural Gas Storage Facilities." https://hifld-geoplatform.opendata.arcgis.com/datasets/geoplatform::natural-gas-storage-facilities/explore?location=31.871965,-98.039391,7.36 (accessed Dec. 22, 2023).

[3] D. Michanowicz, J. Buonocore, S. Rowland, K. Konschnik, S. Goho, and A. Bernstein, "A national assessment of underground natural gas storage: identifying wells with designs likely vulnerable to a single-point-of-failure," *Environmental Research Letters*, vol. 12, no. 6, May 2017, doi: 10.1088/1748-9326/aa7030.

[4] B. Ehrhart, E. Hecht, and B. Schroeder, "Hydrogen Plus Other Alternative Fuels Risk Assessment Models (HyRAM+) Version 5.1 Technical Reference Manual," Sandia National Laboratories, SAND SAND2023-14224, Dec. 2023. [Online]. Available: https://energy.sandia.gov/download/62976/

[5] M. Stephens, "Applying the New PHMSA Guidelines contained in Risk Assessment and Treatment of Wells," presented at the C-FER Technologies Webinar - Part 2, Nov. 17, 2020.

[6] P. A. M. Ujit de Haag and B. J. M. Ale, *Guidelines for quantitative risk assessment ("Purple book")*.

[7] Center for Chemical Process Safety, *Guidelines for Vapor Cloud Explosion, Pressure Vessel Burst, BLEVE, and Flash Fire Hazards*. John Wiley & Sons Ltd., 2010.

[8] "Hydrogen Technologies Code." National Fire Protection Association, 2023.

[9] N. US Department of Commerce, "National Weather Service." https://www.weather.gov/ (accessed Jan. 22, 2024).

[10] L. Pan, C. M. Oldenburg, B. M. Freifeld, and P. D. Jordan, "Modeling the Aliso Canyon underground gas storage well blowout and kill operations using the coupled well-reservoir simulator T2Well," *Journal of Petroleum Science and Engineering*, vol. 161, pp. 158–174, Feb. 2018, doi: 10.1016/j.petrol.2017.11.066.

[11] N. Fisheries, "10 Years of NOAA's Work After the Deepwater Horizon Oil Spill: A Timeline | NOAA Fisheries," *NOAA*, Sep. 26, 2023. https://www.fisheries.noaa.gov/national/habitat-conservation/10-years-noaas-work-after-deepwater-horizon-oil-spill-timeline (accessed Jan. 25, 2024).

[12] Schlumberger, "The SLB Energy Glossary." https://glossary.slb.com/ (accessed Feb. 09, 2024).

[13] "Pipeline Typology and Glossary," Washington Utilities and Transportation Commission, Jun. 2006. [Online]. Available: https://www.utc.wa.gov/sites/default/files/2021-02/LandUseReport-AppendixE-TypologyandGlossary.pdf

[14] M. Portarapillo and A. Di Benedetto, "Risk Assessment of the Large-Scale Hydrogen Storage in Salt Caverns," *Energies*, vol. 14, no. 10, Art. no. 10, Jan. 2021, doi: 10.3390/en14102856.

[15] K. Muhlbauer, *Pipeline Risk Management Manual*, 3rd ed. 2004. [Online]. Available: https://www.sciencedirect.com/book/9780750675796/pipeline-risk-management-manual

[16] "Root Cause Analysis for Aliso Canyon Finalized; California to Continue Strengthening Safeguards for Natural Gas Storage Facilities," California Public Utilities Commission and Department of Conservation. [Online]. Available: https://docs.cpuc.ca.gov/PublishedDocs/Published/G000/M292/K947/292947433.PDF

[17] A. Tchouvelev, “Knowledge gaps in hydrogen: A white paper,” International Energy Agency Hydrogen Implementing Agreement Task 19, Jan. 2008.
[18] J. LaChance, A. Tchouvelev, and A. Engebo, “Development of uniform harm criteria for use in quantitative risk analysis of the hydrogen infrastructure,” *International Journal of Hydrogen Energy*, vol. 36, no. 3, pp. 2381–2388, Feb. 2011, doi: 10.1016/j.ijhydene.2010.03.139.
[19] “Background | Aliso Canyon Disaster Health Research Study.” http://publichealth.lacounty.gov/eh/healthresearch/background.htm (accessed Jan. 04, 2024).
[20] A. R. Cole *et al.*, “Safety of Prolonged Inhalation of Hydrogen Gas in Air in Healthy Adults,” *Crit Care Explor*, vol. 3, no. 10, p. e543, Oct. 2021, doi: 10.1097/CCE.0000000000000543.
[21] H. Djizanne, B. Brouard, P. Berest, G. Hevin, and C. Murillo Rueda, “Blowout from a hydrogen storage cavern,” HAL, Sep. 2022.
[22] N. Meeks, “Hydrogen and Energy Storage,” Nov. 05, 2019. [Online]. Available: https://www.energy.gov/sites/prod/files/2020/01/f70/fcto-fcs-h2-scale-2019-workshop-19-meeks.pdf
[23] Gaffney Cline, “Underground Hydrogen Storage,” Gaffney Cline, 2022. [Online]. Available: https://www.gaffneycline.com/sites/g/files/cozyhq681/files/2022-07/gaffneycline_underground_hydrogen_storage_article.pdf
[24] Air Liquide USA, “H2 Industry.” https://usa.airliquide.com/sustainability/hydrogen/h2-industry (accessed Jan. 30, 2024).
[25] D. Brooks, M. Louie, and B. Ehrhart, “Updated Filter Leak Frequencies for Use in Risk Assessments,” Sandia National Laboratories, In Preparation.

Appendix A. Current Subsurface Hydrogen Storage Landscape

Table A-1. Current Subsurface Hydrogen Storage Facilities in Salt caverns in the United States

Facility Name	**Location** [21]	**Starting Year**	**Owner/Operator** [22]	**Geometric Volume (m^3)** [22]	**Pressure Limits (bar)** [23]
Clemens Dome	Lake Jackson, TX	1983 [22]	Conoco Philips	580,000	70–135
Moss Bluff	Liberty County, TX	2007 [22]	Praxair	566,000	76–134
Spindletop Dome	Beaumont, TX	Commissioned 2017 [24]	Air Liquide	906,000	Information not available

Appendix B. Risk Assessment Inputs and Data

B.1 Model Inputs

The HyRAM+ default ignition probabilities based on leak rates of hydrogen are used to determine immediate ignition probability (associated with jet fires) and delayed ignition probability (associated with explosions) below. These defaults are shown in the table provided. Although there is uncertainty associated with these probabilities, they provide a starting point for risk and other calculations.

Table A-1. Default Ignition Probabilities Used in Risk Assessment [4]

Hydrogen Release Rate (kg/s)	Immediate Ignition Probability	Delayed Ignition Probability
<0.125	0.008	0.004
0.125-6.25	0.053	0.027
>6.25	0.230	0.120

As a comparison, the default HyRAM+ ignition probabilities used in this study are slightly different from those used in the paper by Portarapillo et al. [14], which suggested an immediate ignition probability of 0.1 for the rupture of a vertical riser pipe at the ground and a probability of 0.81 for delayed ignition. The HyRAM+ immediate ignition probability is slightly higher, and the delayed ignition probability is much lower than those reported in the Portarapillo study. Ignition probabilities in general are highly uncertain but can at least be used as a baseline for performing risk assessments and gaining a general understanding of potential leak outcomes.

Other models and values used in the risk assessment are listed in Table A-2 below. Many of these assumptions were default models and values from HyRAM+ [4].

Table A-2. Assumptions Used in Risk Assessment

Input	Model or Value
Thermal harm probit model	Eisenberg
Overpressure harm probit model	The Netherlands Organisation for Applied Scientific Research head impact
Notional nozzle model	Yüceil and Ötügen
Probability of leak detection and isolation	90%
Discharge coefficient from leak	1

Appendix C. Risk Assessment Inputs and Data

C.1 Component Counts

The component counts for reservoir and cavern wellhead configurations are provided in the following tables.

Table B-1. Component Summary for Reservoir Wells

	Component					
Configuration	**Wellhead**	**Surface Casing**	**Production Casing**	**Tubing**	**Packer**	**DHSV**
R1	✓	✓	✓			
R2	✓	✓	✓	✓	✓	
R3	✓	✓	✓	✓	✓	✓

Table B-2. Component Summary for Cavern Wells

	Component				
Configuration	**Wellhead**	**Surface Casing**	**Production Casing**	**Intermediate Casing**	**Tubing**
C1	✓	✓	✓		
C2	✓	✓	✓	✓	
C3	✓	✓	✓	✓	✓

The component count used for the generic aboveground processing facility is shown in the table below.

Table B-3. Component Count for Aboveground Processing Facility

Component	**Number**
Filter	2
Compressor	1
Valve	10
Instrument	5
Joint	10
Pipe	10 (m)

C.2 Failure Frequency Data

C.2.1 Wellhead Operational Failure Frequencies

The fault trees for wellhead operational failure pathways were not explicitly provided in [5], so they were generated using the given diagrams in [5]. To ensure that the fault trees matched the intended failure pathways in [5], the calculated leak frequencies from the fault trees were compared to the reported overall leak frequencies for each wellhead configuration.

Table B-4 below shows annual component failure frequencies from [5].

Table B-4. Total Failure Frequency per Component Provided in [5]

Wellhead Component	Failure Frequency (per Year)
Surface Casing	8.00E-06
Production Casing (above surface casing shoe)	8.00E-06
Intermediate Casing (above surface casing shoe)	8.00E-06
Production Casing (below surface casing shoe)	7.20E-05
Intermediate Casing (below surface casing shoe)	7.20E-05
Wellhead Assembly	5.40E-05
Tubing	2.30E-05
Packer	2.90E-03
DHSV	2.00E-05

The wellhead configuration diagrams were used to determine leak pathways. For example, the R1 configuration includes a wellhead assembly, production casing, and surface casing. The hypothesized leak pathways were through just the wellhead assembly, through the production casing below the surface casing shoe, or through both the production casing above the surface casing shoe and the surface casing. A graphical representation of these leak pathways is provided in the Table A-1 fault tree.

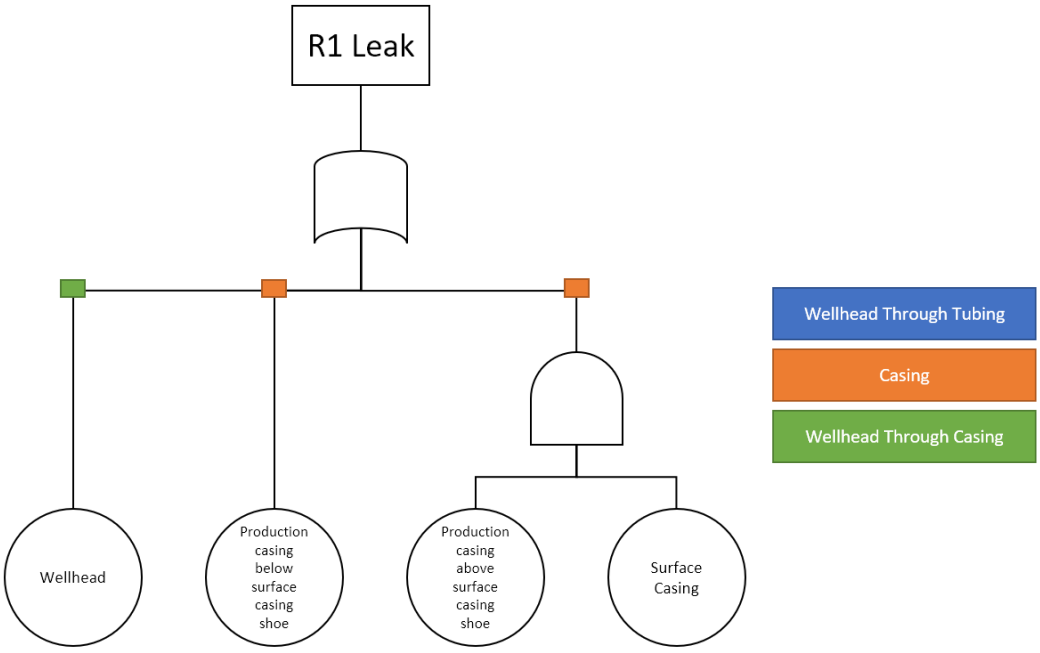


Figure B-1. Complete fault tree for leak pathways in wellhead configuration R1, including releases into the subsurface.

The total leak frequency for the well was calculated by multiplying the leak frequencies of components connected by an “and” gate and adding the leak frequencies of components and pathways connected by an “or” gate. The calculated overall leak frequencies for all wellhead configurations from this method are

shown in the second column of Table B-5. The reported overall leak frequencies for all wellhead configurations from [5] are shown in the third column of the same table.

Table B-5. Percent Error Between Calculated and Reported Total Leak Frequencies by Wellhead Configuration

Wellhead Configuration	Calculated Leak Frequency from Hypothesized Fault Tree	Reported Total Leak Frequency (per Year)	Calculated Result Percent Error from Reported Result
R1	1.26E-04	1.30E-04	-3%
R2	5.40E-05	5.40E-05	0%
R3	3.66E-07	3.70E-07	-1%
C1	1.26E-04	1.30E-04	-3%
C2	5.40E-05	5.40E-05	0%
C3	5.40E-05	5.40E-05	0%

The fourth column of Table B-5 shows the percent error between the leak frequency calculated from the hypothesized fault trees and the leak frequency reported in the data set. A fault tree that led to an overall leak frequency within 5% of the reported overall leak frequency was found for each wellhead configuration. Once these fault trees were generated, they were modified to only include leak pathways to the outside air. For example, in the R1 configuration, only the wellhead assembly leak led to the release of stored fuel into the atmosphere, while the other pathways led to a leak in the subsurface; the subsurface leak pathways were removed from the fault trees, which are shown below for each configuration. Note that the fault trees are valid for any size of leak to the atmosphere.

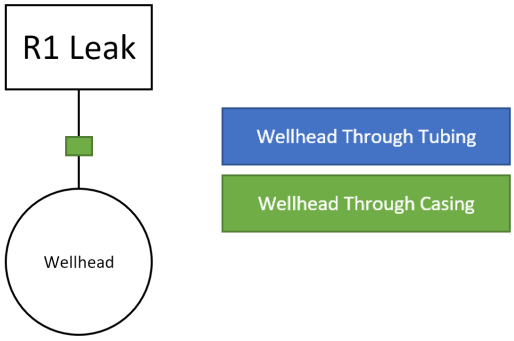


Figure B-2. Fault tree for configuration R1.

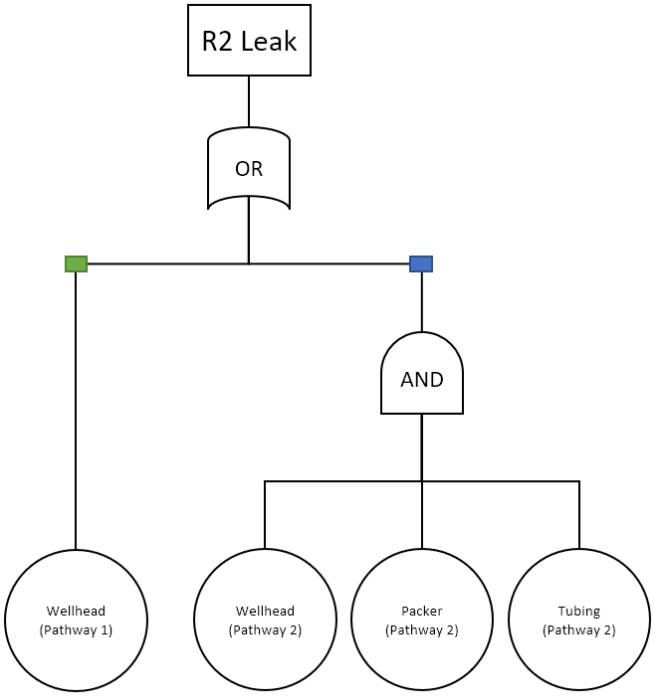


Figure B-3. Fault tree for configuration R2.

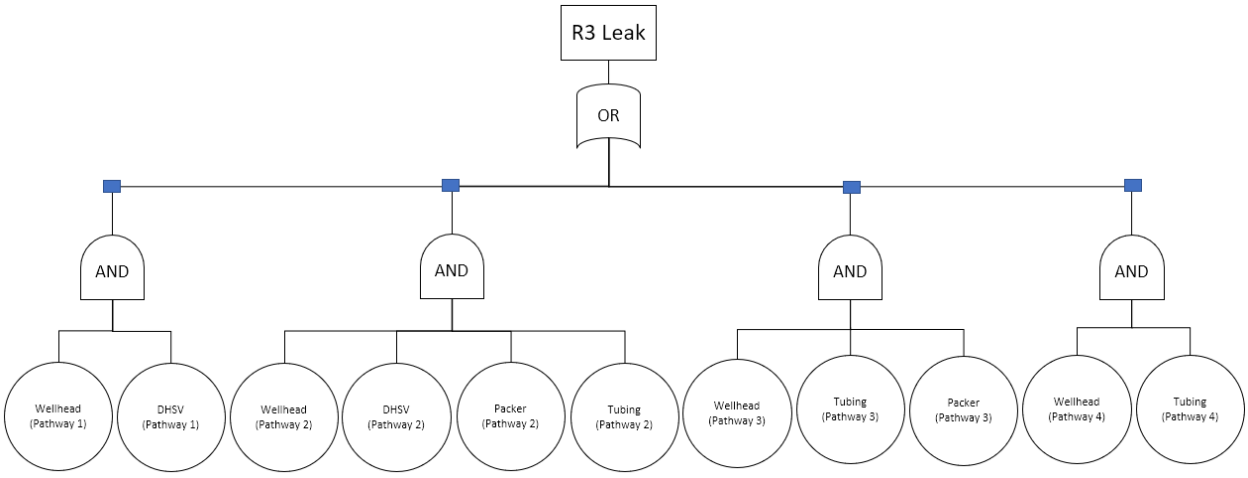


Figure B-4. Fault tree for configuration R3.

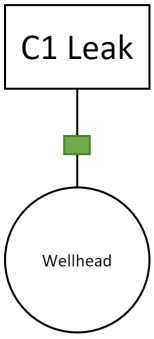


Figure B-5. Fault tree for configuration C1.

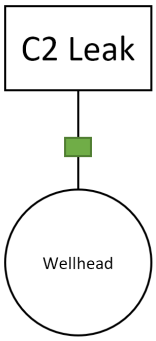


Figure B-6. Fault tree for configuration C2.

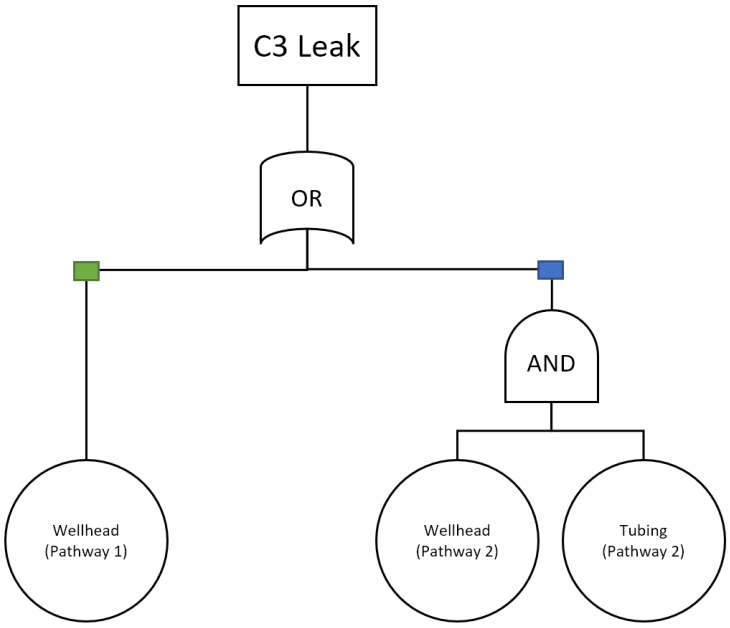


Figure B-7. Fault tree for configuration C3.

The data source also provided a breakdown of the likelihood of different leak sizes in each component, shown in Table B-6.

Table B-6. Likelihood of Leaks per Component by Leak Size from [5]

Component	Failure Mode Likelihood		
	Small Leak	Large Leak	Rupture
Surface Casing	83%	12%	5%
Production Casing (above surface casing shoe)	83%	12%	5%
Intermediate Casing (above surface casing shoe)	83%	12%	5%
Production Casing (below surface casing shoe)	83%	12%	5%
Intermediate Casing (below surface casing shoe)	83%	12%	5%
Wellhead Assembly	79%	17%	4%
Tubing	91%	7%	2%
Packer	85%	10%	5%
DHSV	0%	56%	44%

Like the ignition probabilities used in this study, leak frequencies are highly uncertain, especially for hydrogen since the available historical data is generally from the oil and gas industry and may not be accurate for hydrogen systems. The paper by Portarapillo et al. considers that a rupture of a vertical riser pipe at the ground for an underground hydrogen system would occur with a frequency of around 6.5×10^{-5} times per year. This is on the same order of magnitude as the total failure frequency of the wellhead assembly component reported by Stephens in the data set used in this report (see Table B-4) [5]; however, the rupture-specific leak in the wellhead assembly only happens around 4% of that time (see Table B-6). Still, it is helpful to see that the leak frequencies used in this report are not drastically different from those reported elsewhere in literature.

C.2.2 Wellhead Entry Failure Frequencies

This section includes data from [5] used to calculate annual leak frequencies for each well entry type and leak size. Figure B-8 shows the annual frequency of each type of well entry (wireline, coiled tubing, and workover) for each well configuration. This data was used with Table B-7 to break down annual well entry failures by entry type and Table B-8 to further parse out annual failures by leak size. Table B-9 contains a summary of annual failures by well entry type and leak size.

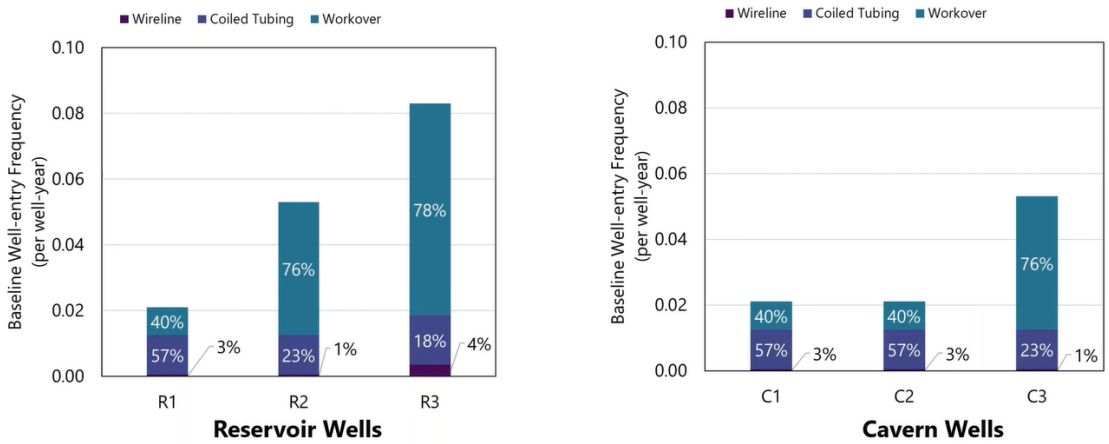


Figure B-8. Frequency of well entries for each well configuration by well entry type [5].

Table B-7. Well Entry Failure Rates [5]

Well Entry Type	Failure Rate per Entry
Workover	2.0E-04
Coiled Tubing	5.5E-05
Wireline	4.5E-06

Table B-8. Breakdown of Well Entry Leak Sizes [5]

Leak Size	Percentage of Well Entry Leaks
Small	9%
Large	73%
Rupture	18%

Table B-9. Annual Frequency of Well Entry Failures by Type and Leak Size

Well Configuration	Annual Well Entries	Annual Well Entry Failures								
		Workover			Coiled Tubing			Wireline		
		Small	Large	Rupture	Small	Large	Rupture	Small	Large	Rupture
R1	0.021	1.5E-07	1.2E-06	3.0E-07	5.9E-08	4.8E-07	1.2E-07	2.6E-10	2.1E-09	5.1E-10
R2	0.0529	7.2E-07	5.9E-06	1.4E-06	6.0E-08	4.9E-07	1.2E-07	2.1E-10	1.7E-09	4.3E-10
R3	0.0831	1.2E-06	9.5E-06	2.3E-06	7.4E-08	6.0E-07	1.5E-07	1.3E-09	1.1E-08	2.7E-09
C1	0.021	1.5E-07	1.2E-06	3.0E-07	5.9E-08	4.8E-07	1.2E-07	2.6E-10	2.1E-09	5.1E-10
C2	0.021	1.5E-07	1.2E-06	3.0E-07	5.9E-08	4.8E-07	1.2E-07	2.6E-10	2.1E-09	5.1E-10
C3	0.053	7.3E-07	5.9E-06	1.5E-06	6.0E-08	4.9E-07	1.2E-07	2.1E-10	1.7E-09	4.3E-10

C.2.3 Aboveground Processing Facility Operational Failure Frequencies

Table B-10 shows annual leak frequencies for different sized leaks from the aboveground processing facility. These leak frequencies were all taken from the default leak data provided in the 2023 version of HyRAM+ except for the filter leak frequencies, which were concurrently being documented and updated at the time this report was being written [25].

Table B-10. Annual Leak Frequency per Component in Aboveground Processing Facility by Size [4]

Component	Leak Size (Percentage of Pipe Area)				
	0.01%	0.1%	1%	10%	100%
Filter	2.97E-03	9.98E-04	3.35E-04	1.17E-04	3.72E-05
Compressor	9.97E-02	1.70E-02	4.57E-03	1.52E-04	1.46E-05
Valve	2.87E-03	5.86E-04	5.44E-05	2.47E-05	4.82E-06
Instrument	6.24E-04	1.95E-04	1.12E-04	1.00E-04	3.68E-05
Joint	3.50E-05	4.69E-06	7.86E-06	7.53E-06	6.40E-06
Pipe	8.02E-06	3.70E-06	9.56E-07	4.61E-07	1.47E-07

The fault tree for the processing facility is shown below in Figure B-9.

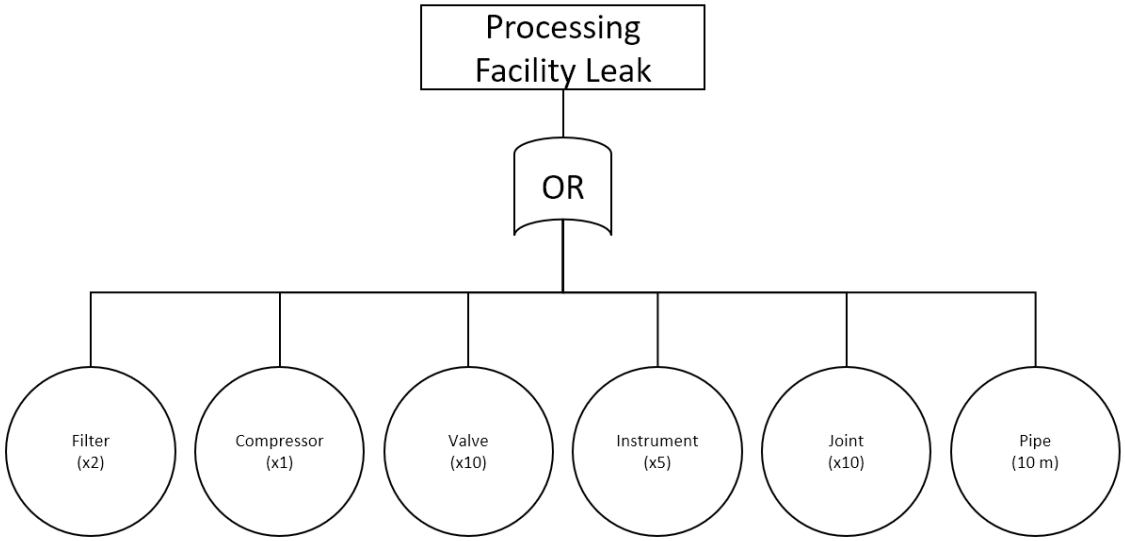


Figure B-9. Fault tree for aboveground processing facility.

C.3 Leak Sizes

C.3.1 Wellhead Failure Leak Sizes

Table B-11 shows orifice sizes for each type of wellhead leak point. The leak diameters were provided in [5] for each leak size. The leak size as a percentage of the cross-sectional area of the leaking component was computed for easy comparison with leak sizes in the aboveground processing facility because leak size qualifiers such as “small,” “large,” and “rupture” had inconsistent meanings across the datasets used for the wellhead and processing facility leak sizes.

Table B-11. Wellhead Leak Sizes

Facility	Leaking Component	Leaking Component Diameter (mm)	Leak Diameter (mm)		Percentage of Component Area
Wellhead	Wellhead through Tubing	114	Small	1	0.01
			Large	11	1
			Rupture	110	93
	Wellhead through Casing (Production, Intermediate, or Surface)	178, 273, 273	Small	2	0.01, <0.01, <0.01
			Large	18	1, 0.4, 0.4
			Rupture	180	100, 43, 43

C.3.2 Aboveground Processing Facility Leak Sizes

The leak sizes for the aboveground processing facility were based on the HyRAM+ methodology of using five leak sizes, given as a percentage of cross-sectional area rather than as an absolute diameter or area [4].

Table B-12. Aboveground Processing Facility Leak Sizes

Facility	Leaking Component Diameter (mm)	Leak Diameter (mm)		Percentage of Component Area
Processing Facility	180	Very Small	1.8	0.01
		Minor	5.7	0.1
		Medium	18	1
		Major	56.9	10
		Rupture	180	100

Appendix D. Mesh Size Study for Societal Risk Calculations

HyRAM+ can be used calculate metrics such as probability of fatality and risk at a single point, but the societal risk calculations require the consideration of an area as a location of interest since societal or population density is inherently area-based. However, physical effects of a leak such as heat flux from a jet fire or overpressure from an explosion vary over space. Therefore, calculating the probability of fatality at multiple points and taking the average (Equation 2-2), is helpful for improving the accuracy of fatality calculations.

Selecting a number of points for these calculations requires several considerations. The sampled points should not be too far from each other because they may fail to capture significant changes in fatality probability that occur between them. They should also not be too close because calculations become more computationally expensive from a time perspective and orders of magnitude smaller than on the order of feet (or tenths of meters) are not of interest for this application, since the cells defined by the points should be large enough to fully contain a person.

A mesh size study was conducted to assist with the selection of the number and locations of calculation points in the area of interest. The area of interest was 50 m by 50 m, and the largest mesh size used is shown in

Figure C-10(a), with a calculation every 10 meters in the x direction (parallel to the leak) and the z direction (perpendicular to the leak). The calculation interval was halved until reaching a mesh with a calculation interval of 0.625 m.

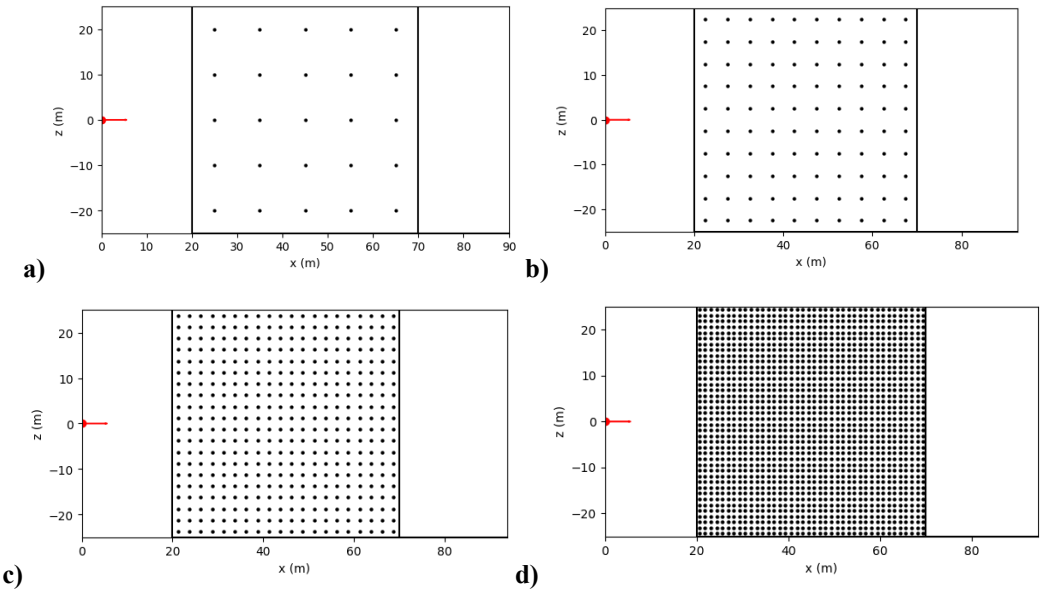


Figure C-10. Area of interest with a sample location a) every 10 m, b) every 5 m, c) every 2.5 m, and d) every 1.25 m.

The total number of fatalities in the area of interest, as a percentage of the total population in the area, was calculated for each leak size from the processing facility and wellhead, for each mesh size. These results are shown below in Table C-13.

Table C-13. Number of Fatalities in Area of Interest with 2700 People per Square Mile

Sampling Interval (m)	Processing Facility Leak Diameters (mm)					Wellhead Through Tubing Leak Diameters (mm)			Wellhead Through Casing Leak Diameters (mm)		
	1.8	5.7	18	56.9	180	1	11	110	2	18	180
10	0	0	0	1.2	2.6	0	0.4	2.6	0	0	2.6
5	0	0	0	1.3	2.6	0	0.3	2.6	0	0.01	2.6
2.5	0	0	0	1.3	2.6	0	0.3	2.6	0	0.02	2.6
1.25	0	0	0	1.3	2.6	0	0.3	2.6	0	0.02	2.6
0.625	0	0	0	1.3	2.6	0	0.3	2.6	0	0.02	2.6

The absolute differences between the total number of fatalities calculated from each mesh and the previous mesh size are shown below in Table C-14.

Table C-14. Absolute Difference in Number of Fatalities Between Each Mesh Size and Its Previous Mesh Size

Sampling Interval (m)	Processing Facility Leak Diameters (mm)					Wellhead Through Tubing Leak Diameters (mm)			Wellhead Through Casing Leak Diameters (mm)		
	1.8	5.7	18	56.9	180	1	11	110	2	18	180
10	-	-	-	-	-	-	-	-	-	-	-
5	0	0	1.3E-05	1.3E-02	2.9E-05	0	2.4E-02	1.3E-08	0	1.3E-02	4.4E-06
2.5	0	0	2.5E-04	1.3E-03	1.3E-05	0	1.8E-03	8.6E-09	0	4.4E-03	2.2E-06
1.25	0	0	2.9E-04	3.5E-04	3.7E-06	0	2.6E-05	2.7E-09	0	1.5E-04	6.5E-07

The absolute differences, or changes between fatality calculations for each mesh size, assisted in the determination of an appropriate mesh to use. Reaching a “small enough” absolute difference would indicate an acceptable mesh, but the definition of “small enough” is application dependent. The leak sizes of interest all led to drastically different fatality numbers, with orders of magnitude ranging from predictions of fatalities in hundreds of orders of magnitude less than 0.01% of the population to fatalities in 100% of the population. Some fatality numbers are already negligible, such as those calculated for the smallest two processing facility leak sizes and the smallest wellhead sizes).

The absolute differences in fatality numbers ended up being very small, with orders of magnitude that were much lower than the orders of magnitude of the fatality numbers themselves. This result indicated that mesh size did not matter much for generating societal risk since making the mesh size finer did not drastically change the fatality numbers. The computational time was reasonable with all mesh sizes tested, with the 1.25 m interval mesh size still only taking around a minute to generate results. The 1.25 m interval mesh size was used for the societal risk study.

Appendix E. Risk Assessment Results

E.1 Societal Risk Results

The societal risk results are provided in this section in terms of the annual frequency of each type of physical consequence from each leak size and the number of calculated fatalities as a percentage of people living in the 50 m x 50 m area shown in Figure 2-2. Table D-15, Table D-16, and Table D-17, correspond to the graphs shown in Figure 4-5, and Figure 4-6.

Table D-15. Societal Risk Results for Wellhead Operational Leaks

Cavern Configuration	Leak Point	Leak Size (m)	Jet Fire		Overpressure	
			Annual Frequency	Number of Fatalities in Area of Interest	Annual Frequency	Number of Fatalities in Area of Interest
R1	WTC	0.002	3.4E-08	0	1.7E-08	0
		0.018	4.9E-08	0.3	2.5E-08	0
		0.18	5.0E-08	2.6	2.6E-08	0.0002
R2	WTC	0.002	3.4E-08	0	1.7E-08	0
		0.018	4.9E-08	0.3	2.5E-08	0
		0.18	5.0E-08	2.6	2.6E-08	0.0002
	WTT	0.001	1.8E-15	0	8.8E-16	0
		0.011	2.3E-17	0.02	1.2E-17	0
		0.11	3.3E-18	2.6	1.7E-18	0
R3	WTT	0.001	7.2E-13	0	3.6E-13	0
		0.011	6.2E-13	0.02	3.2E-13	0
		0.11	4.6E-13	2.6	2.4E-13	0
C1	WTC	0.002	3.4E-08	0	1.7E-08	0
		0.018	4.9E-08	0.3	2.5E-08	0
		0.18	5.0E-08	2.6	2.6E-08	0.0002
C2	WTT	0.001	3.4E-08	0	1.7E-08	0
		0.011	4.9E-08	0.02	2.5E-08	0
		0.11	5.0E-08	2.6	2.6E-08	0
C3	WTC	0.002	3.4E-08	0	1.7E-08	0
		0.018	4.9E-08	0.3	2.5E-08	0
		0.18	5.0E-08	2.6	2.6E-08	0.0002
	WTT	0.001	7.1E-13	0	3.6E-13	0
		0.011	7.8E-14	0.02	4.0E-14	0
		0.11	2.3E-14	2.6	1.2E-14	0

Table D-16. Societal Risk Results for Wellhead Entry Leaks

Cavern Configuration	Leak Size (m)	Jet Fire		Overpressure	
		Annual Frequency	Number of Fatalities in Area of Interest	Annual Frequency	Number of Fatalities in Area of Interest
R1	0.002	1.7E-10	0	8.4E-11	0
	0.018	8.9E-09	0.3	4.6E-09	0
	0.18	9.7E-09	2.6	5.0E-09	0.0002
R2	0.002	6.2E-10	0	3.1E-10	0
	0.018	3.4E-08	0.3	1.7E-08	0
	0.18	3.5E-08	2.6	1.8E-08	0.0002
R3	0.002	1.0E-09	0	5.1E-10	0
	0.018	5.4E-08	0.3	2.7E-08	0
	0.18	5.6E-08	2.6	2.9E-08	0.0002
C1	0.002	1.7E-10	0	8.4E-11	0
	0.018	8.9E-09	0.3	4.5E-09	0
	0.18	9.7E-09	2.6	5.0E-09	0.0002
C2	0.002	1.7E-10	0	8.4E-11	0
	0.018	8.9E-09	0.3	4.5E-09	0
	0.18	9.7E-09	2.6	5.0E-09	0.0002
C3	0.002	6.3E-10	0	3.2E-10	0
	0.018	3.4E-08	0.3	1.7E-08	0
	0.18	3.7E-08	2.6	1.9E-08	0.0002

Table D-17. Societal Risk Results for Aboveground Processing Facility Leaks

Leak Size (m)	Jet Fire		Overpressure	
	Annual Frequency	Number of Fatalities in Area of Interest	Annual Frequency	Number of Fatalities in Area of Interest
1.8E-3	1.8E-03	0	1.1E-05	0
5.7E-3	5.7E-03	0	9.8E-04	0
1.8E-2	1.8E-02	0.001	1.4E-02	0
5.6E-2	5.6E-02	1.3	1.7E-01	0
1.8E-1	1.8E-01	2.6	9.8E-01	0

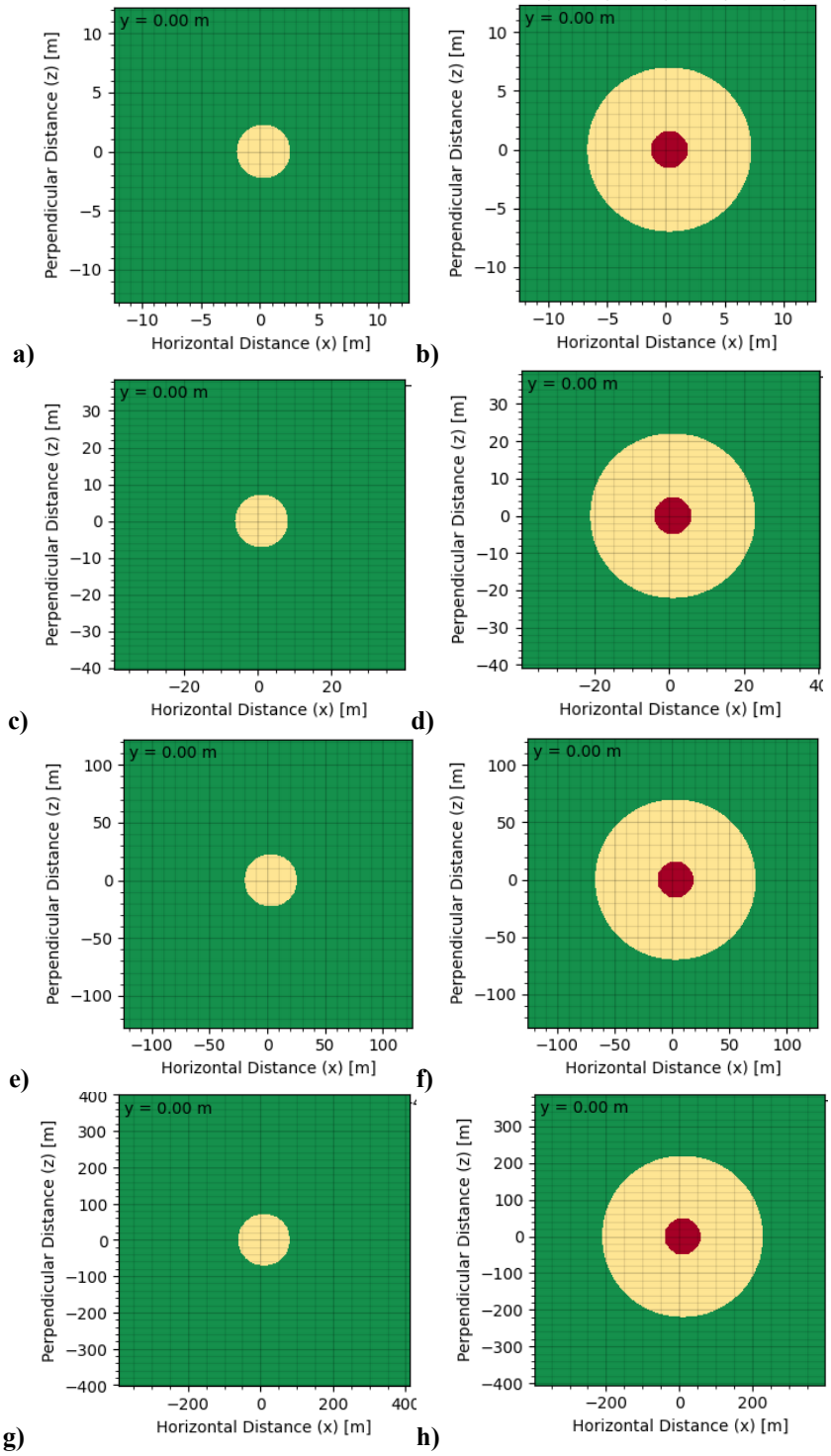
E.2 Sensitivity Study Individual Risk Results

Table D-18. Summary of All Sensitivity Study Conditions

Conditions	Scenarios						
	Default Conditions	**Increased Confinement/ Obstacles**	**Beaumont, TX Summer Ambient Conditions**	**Charleston, WV Summer Ambient Conditions**	**St. Clair, MI Winter Ambient Conditions**	**Allegany, NY Winter Ambient Conditions**	**Adjusted Storage Conditions**
Ambient Temperature (°C)	20	20	44	32	-18	-19	20
Ambient Humidity (%)	89	89	52	90	60	89	89
Storage Temperature (°C)	80	80	80	80	80	80	65
Storage Pressure (MPa)	30	30	30	30	30	30	40
Mach Flame Speed	0.35	5.2	0.35	0.35	0.35	0.35	0.35

Table D-19. Sensitivity Study Individual Risk Results in Fatalities per Year at z=0 (Corresponds to Figure 4-12)

Distance from Leak (m)	**Default Conditions**	**Increased Confinement/ Obstacles**	**Beaumont, TX Summer Ambient Conditions**	**Charleston, WV Summer Ambient Conditions**	**St. Clair, MI Winter Ambient Conditions**	**Allegany, NY Winter Ambient Conditions**	**Adjusted Storage Conditions**
1	2.0E-03	2.5E-03	2.0E-03	2.0E-03	2.0E-03	2.0E-03	2.0E-03
10	7.1E-04	9.0E-04	7.1E-04	7.1E-04	7.1E-04	7.1E-04	7.1E-04
20	4.7E-04	5.7E-04	6.1E-04	5.3E-04	3.7E-04	3.8E-04	4.7E-04
30	3.7E-04	4.1E-04	3.7E-04	3.7E-04	3.7E-04	3.7E-04	3.7E-04
40	3.7E-04	4.1E-04	3.7E-04	3.7E-04	3.7E-04	3.7E-04	3.7E-04
50	3.6E-04	4.1E-04	3.7E-04	3.7E-04	2.9E-04	3.0E-04	3.6E-04
60	1.3E-04	1.7E-04	1.8E-04	1.4E-04	9.4E-05	9.5E-05	1.3E-04
70	8.9E-05	1.4E-04	8.9E-05	8.9E-05	8.9E-05	8.9E-05	8.9E-05
80	8.9E-05	8.9E-05	8.9E-05	8.9E-05	8.9E-05	8.9E-05	8.9E-05
90	8.9E-05	8.9E-05	8.9E-05	8.9E-05	8.9E-05	8.9E-05	8.9E-05
100	8.9E-05	8.9E-05	8.9E-05	8.9E-05	8.9E-05	8.9E-05	8.9E-05


y = 0.00 m
Perpendicular Distance (z) [m]
Horizontal Distance (x) [m]
a)
b)
c)
d)
e)
f)
g)
h)

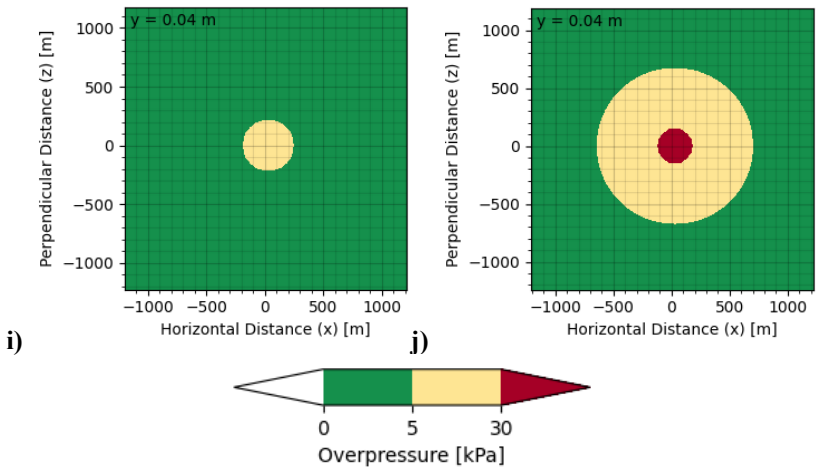


Figure D-11. Overpressure contours for a 0.01% leak (a, b), 0.1% leak (c, d), 1% leak (e, f), 10% leak (g, h), and 100% leak (i, j), where Mach flame speed was set to 0.35 (figures on left) and 5.2 (figures on right).

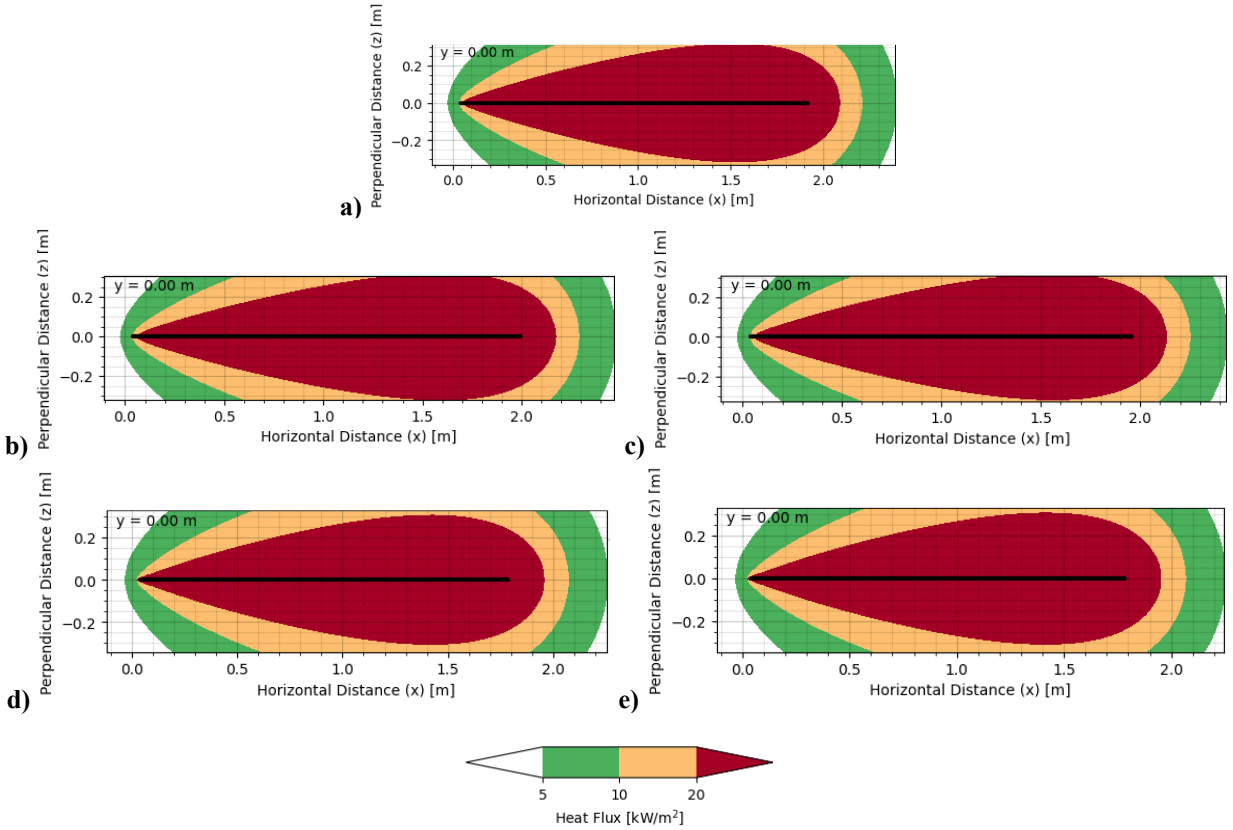


Figure D-12. Heat flux contours for 0.01% leak using a) HyRAM+ default, b) Beaumont, TX summer, c) Charleston, SC summer, d) St. Clair, MI winter, and Allegany, NY winter example ambient conditions.

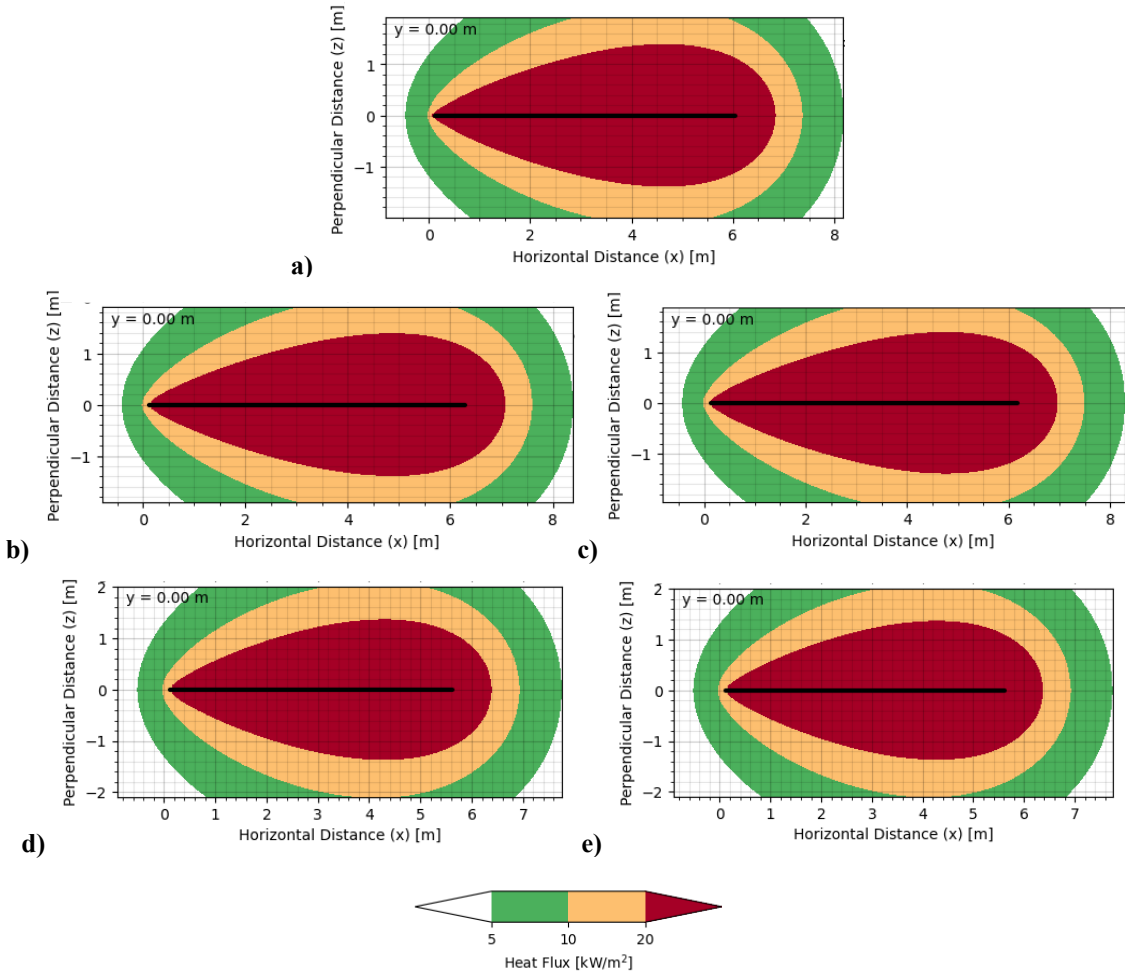


Figure D-13. Heat flux contours for 0.1% leak using a) default, b) Beaumont, TX summer, c) Charleston, SC summer, d) St. Clair, MI winter, and Allegany, NY winter example ambient conditions.

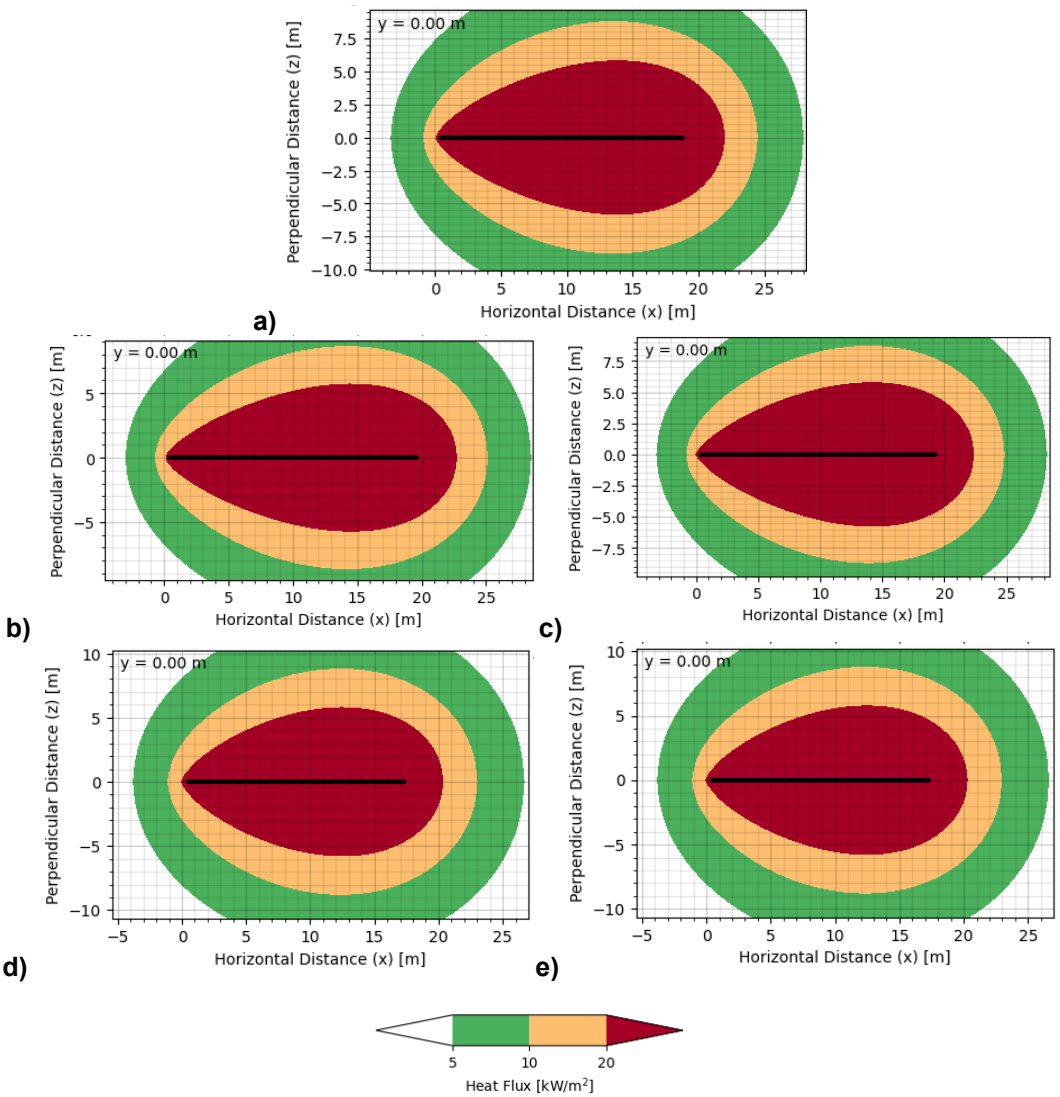


Figure D-14. Heat flux contours for 1% leak using a) default, b) Beaumont, TX summer, c) Charleston, SC summer, d) St. Clair, MI winter, and Allegany, NY winter example ambient conditions.

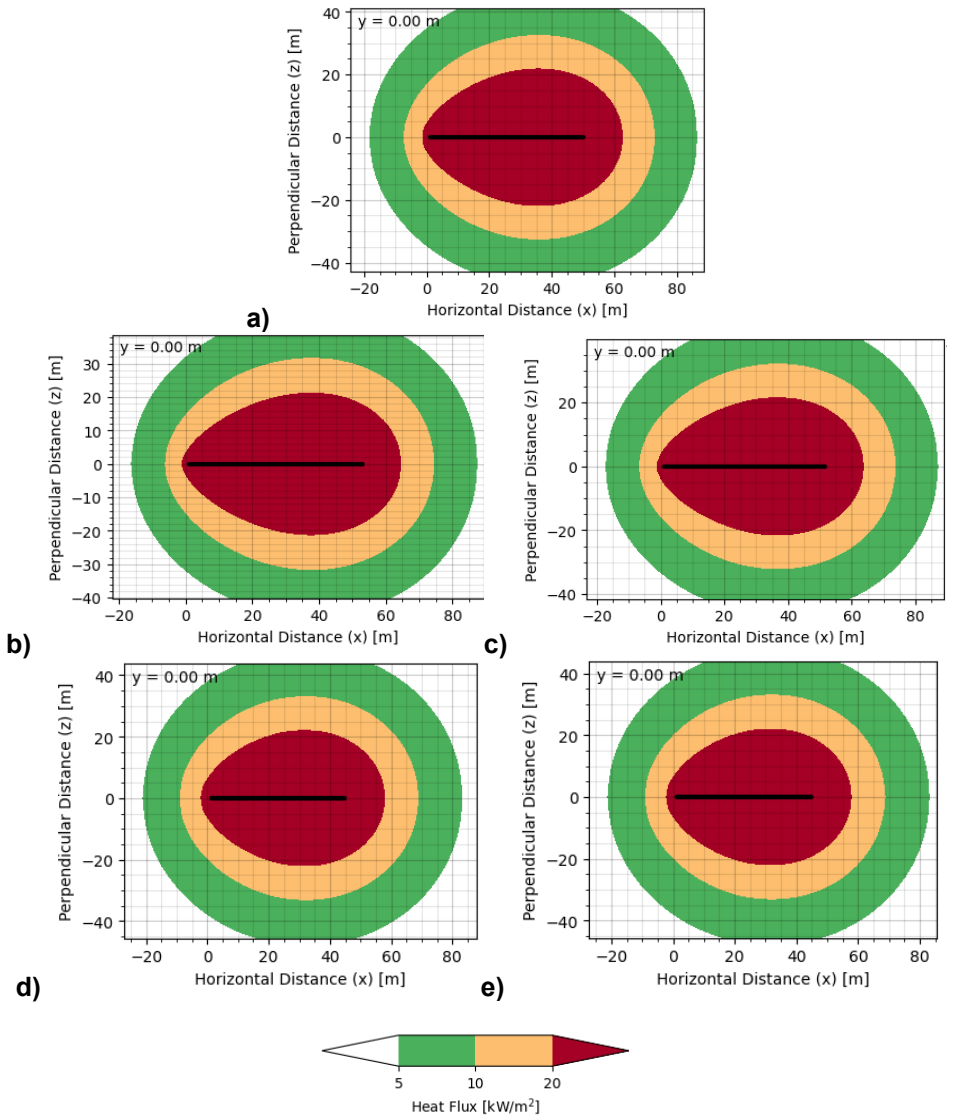


Figure D-15. Heat flux contours for 10% leak using a) default, b) Beaumont, TX summer, c) Charleston, SC summer, d) St. Clair, MI winter, and Allegany, NY winter example ambient conditions.

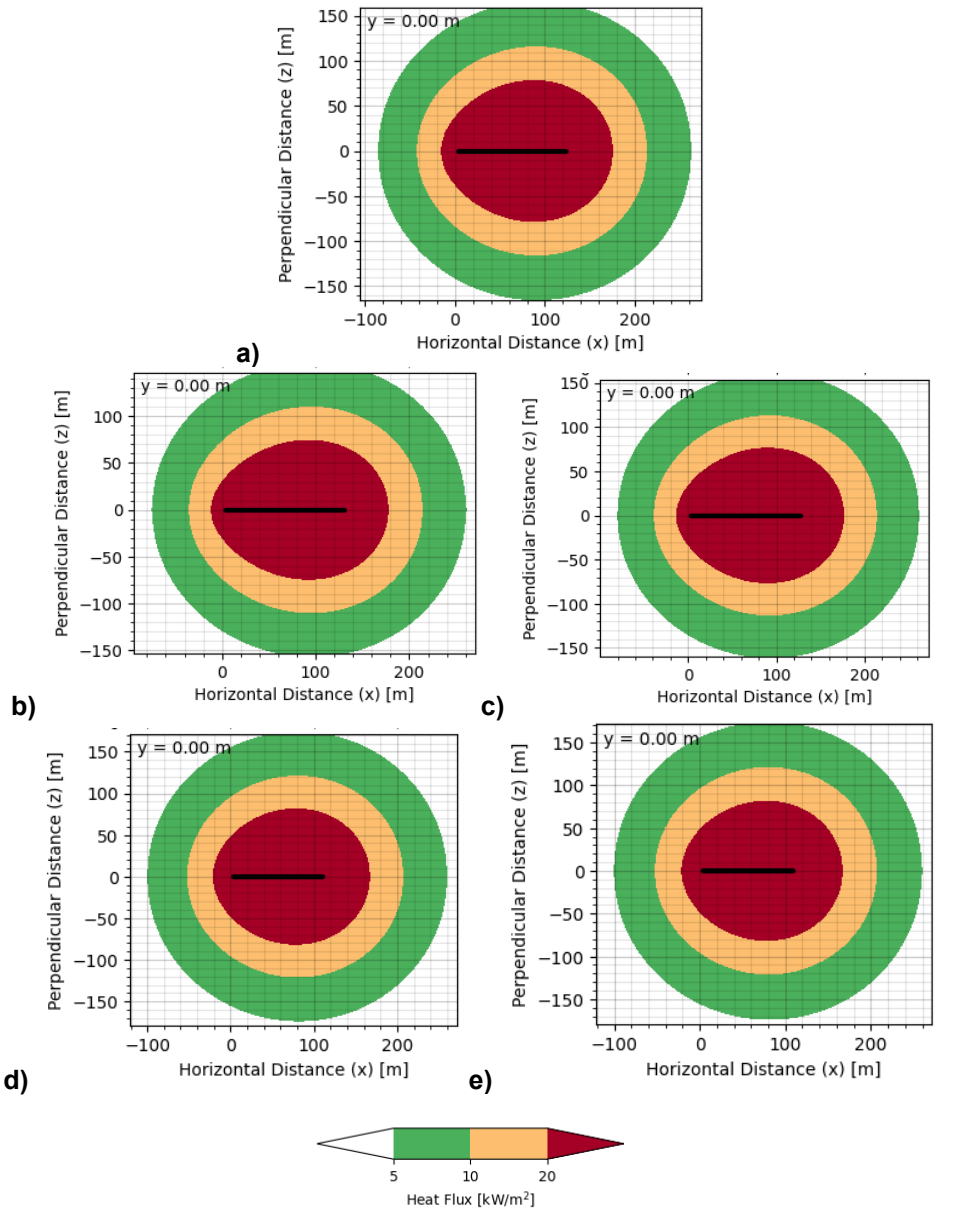


Figure D-16. Heat flux contours for 100% leak using a) default, b) Beaumont, TX summer, c) Charleston, SC summer, d) St. Clair, MI winter, and Allegany, NY winter example ambient conditions.

Contacts

Evan Frye
Natural Gas Decarbonization and Hydrogen Technologies Program Manager
Office of Fossil Energy and Carbon Management (FECM) – Office of Resources Sustainability
U.S. Department of Energy
evan.frye@hq.doe.gov

Timothy Reinhardt
Director – Division of Methane Mitigation Technologies
Office of Fossil Energy and Carbon Management (FECM) – Office of Resources Sustainability
U.S. Department of Energy
timothy.reinhardt@hq.doe.gov

Bill Fincham
Technology Manager
National Energy Technology Laboratory
william.fincham@netl.doe.gov

Angela Goodman
SHASTA Technical Lab Lead, PI
National Energy Technology Laboratory
angela.goodman@netl.doe.gov

Nicolas Huerta
SHASTA Technical Lab Lead, co-PI
Pacific Northwest National Laboratory
nicolas.huerta@pnnl.gov

Joshua White
SHASTA Technical Lab Lead, co-PI
Lawrence Livermore National Laboratory
white230@llnl.gov

Mathew Ingraham
SHASTA Technical Lab Lead, co-PI
Sandia National Laboratories
mdingr@sandia.gov